Type I interferon expression requires transcriptional activation of IRF7 by the RNA binding protein SRSF7

Haley M. Scott[1], Mackenzie H. Smith[1], Aja K. Coleman[1], Allison R. Wagner[1,2], Robert O. Watson[1], Kristin L. Patrick[1*#]

[1]Department of Microbial Pathogenesis and Immunology, Texas A&M University School of Medicine

[2]Department of Immunology, UT Southwestern Medical Center

*Corresponding author: kpatrick03@tamu.edu

#Lead contact

Phone: (979) 436-0354

Twitter: @The_PW_Lab

Abstract

While the signaling cascades and transcription factors that turn on expression of innate immune genes are well-characterized, the role of RNA binding proteins in activating and sustaining the innate immune response is poorly understood. Members of the serine/arginine-rich (SR) family of mRNA processing factors play diverse roles in transcription, pre-mRNA splicing, export, and translation. Transcriptomic analysis of murine macrophage cell lines revealed that one such SR protein, SRSF7, is required for optimal expression of interferon stimulated genes (ISGs) at rest and in response to a variety of innate immune stimuli in a splicing-independent fashion. We demonstrate that SRSF7 is necessary and sufficient to drive expression of interferon regulatory transcription factor 7 (IRF7), an important activator of the type I IFN response in resting and LPS-treated macrophages. By associating with the *Irf7* promoter, SRSF7 maximizes binding of the STAT1 transcription factor and promotes RNA polymerase II elongation. These studies define an unorthodox role for an SR protein in activating transcription and highlight the importance of RNA binding proteins in shaping the macrophage innate immune response to pathogens.

68 **Introduction**

69 In mammals, the SR (serine-arginine rich) family of proteins is comprised of >10 RNA
70 binding proteins that are broadly defined as regulators of alternative splicing. By virtue of distinct
71 RNA recognition motifs, SRs bind to unique exonic splicing enhancers to help direct the spliceo-
72 some to cis-splicing signals in target transcripts (Wagner and Frye, 2021). While best known for
73 their role in pre-mRNA splicing, SRs can participate in virtually any step of RNA processing, from
74 transcription all the way to translation (Jeong, 2017). To date, studies of SR function have mostly
75 been carried out in genetically tractable "model" cell lines (e.g. K562, HEK293T, and HepG2), but
76 there is a growing appreciation for the importance of SR proteins in responding to stress and
77 shaping the transcriptome in specialized cell types. Specialization of SR protein function has been
78 repeatedly linked to post-translational modification, which can alter the subcellular localization,
79 protein binding partners, and RNA recognition abilities of SRs, ultimately enabling them to carry
80 out different functions in different cell types (Colwill et al., 1996; Duncan et al., 1995; Gui et al.,
81 1994).

82 We are just beginning to appreciate the potential roles for SR protein functionalization in
83 immune cells. Recent proteomics analyses identified multiple SR proteins that are differentially
84 phosphorylated in macrophages upon infection with intracellular pathogens like the bacterium
85 *Mycobacterium tuberculosis* (Budzik et al., 2020) and the fungal pathogen *Cryptococcus neofor-*
86 *mans* (Pandey et al., 2017). Macrophages (MΦ) are innate immune cells that serve as the body's
87 first line of defense against pathogens. They express a variety of extracellular, endosomal, and
88 cytosolic pattern recognition receptors that detect pathogen- and damage-associated molecular
89 patterns (PAMPs and DAMPs) and transmit these "danger signals" to the nucleus though complex
90 signal transduction cascades. Activation of these cascades turns on expression of hundreds of
91 cytokines, chemokines, and antimicrobial mediators, many of which are transcriptionally and
92 translationally upregulated >100-fold in a matter of minutes (Nau et al., 2002). While a rapid and
93 robust innate immune response is needed to limit infection, a response that is too strong carries
94 risks (e.g. cytokine storm, autoimmunity, chronic inflammation, etc.). Therefore, MΦ gene expres-
95 sion needs to be tightly regulated. Despite their critical role in shaping mammalian transcriptomes,
96 molecular mechanisms though which SR proteins regulate macrophage gene expression—both
97 in terms of maintaining homeostatic levels of antimicrobial mediators and in inducing innate genes
98 following a stimulus—remain poorly understood.

99 We hypothesized that SR proteins with the potential to undergo modification downstream
100 of pattern recognition receptor engagement play a privileged role in tuning the macrophage re-
101 sponse to pathogens. We found that stable knockdown of several of these SR proteins in RAW

264.7 macrophage-like cells (RAW MΦs) profoundly altered the macrophage transcriptome in resting and activated macrophages (4h post-*Salmonella* Typhimurium infection) (Wagner et al., 2021). The absence of one of these proteins, SRSF7, generated some particularly interesting phenotypes. SRSF7 (formerly known as 9G8) is a canonical member of the SR protein family. It encodes an RNA recognition motif (RRM) and an eponymic SR domain. It is the only SR family protein to also encode a CCHC-type Zn knuckle domain, which is thought to contribute to its RNA-binding specificity (Cavaloc et al., 1999; Cavaloc et al., 1994; Wang et al., 2021)). To date, its function is best studied in the context of mRNA export (Muller-McNicoll et al., 2016) and in controlling its own expression levels via poison cassette exon inclusion (Konigs et al., 2020).

In RAW MΦs lacking SRSF7, we identified a large cohort of transcripts whose alternative splicing (AS) was dependent on SRSF7. We also identified genes whose expression relied on SRSF7 at rest and after *Salmonella* infection. Curiously, in both conditions, many SRSF7-impacted genes fell into the category of interferon stimulated genes (ISGs). Studies suggest that as much as 10% of the human genome has the potential to be regulated by one of the three types of IFNs (I, II, III). Macrophages robustly express type I IFNs and hundreds of ISGs in response to innate stimuli like lipopolysaccharide (LPS) and cytosolic nucleic acids. After ruling out a role for SRSF7 in alternative splicing of these ISGs, we set out to elucidate the mechanism though which SRSF7 controls the type I IFN response in macrophages. We report a novel role for SRSF7 in controlling the abundance of interferon responsive factor 7 (IRF7), a critical player in activating the type I IFN response (Ning et al., 2011). Specifically, we demonstrate that SRSF7 promotes *Irf7* transcription by enabling recruitment of signal transducer and activator of transcription 1 (STAT1) to the *Irf7* promoter and relieving RNAPII pausing. Together, these data identify SRSF7 as a transcriptional activator and provide important insight into how SR proteins can regulate innate immune responses in macrophages in unexpected ways.

Results

SRSF7 control of alternative splicing is independent of macrophage activation state

Motivated by aforementioned phosphoproteomics analyses (Budzik et al., 2020; Pandey et al., 2017) and previous studies of hnRNP M (West et al., 2019) and SRSF6 (Wagner et al., 2022), we sought to identify additional splicing regulatory proteins that are functionally regulated in the context of macrophage activation. To test the hypothesis that AS events might be distinct between resting and activated macrophages, signifying functionalization of SRSF7, we generated two *Srsf7* knockdown cell lines by transducing RAW 264.7 MΦs (*Srsf7* KD #1 and *Srsf7* KD #2) with lentivirus containing shRNA hairpin constructs designed against the *Srsf7* 3'UTR. These cell lines were selected alongside a scramble (SCR) control. We generated macrophage cell lines

with stable knockdown of *Srsf7* at the RNA (**Fig. 1A**) and protein level (**Fig. 1B**) with ~70-80% efficiency. We performed RNA-seq (150 bp paired-end reads; Illumina 4000; ~20 million reads per sample in triplicate) on RNA isolated from *Srsf7* KD #2 and SCR control cells that were resting (uninfected; UN) or infected with the gram-negative bacterial pathogen *Salmonella enterica* serovar Typhimurium (4h post-infection; +SAL). *Salmonella* induces robust innate immune responses in macrophages though TLR4, which activates NFκB downstream of the MyD88 adapter and IRF3/IRF7 downstream of TRIF (Fitzgerald et al., 2003). Differential expression analysis was conducted using the Qiagen CLC Genomics Workbench and quantification of alternative splicing changes was carried out using MAJIQ (Modeling Alternative Junction Inclusion Quantification) (Vaquero-Garcia et al., 2016). Consistent with SRSF7's designation as a splicing factor and previous studies implicating it in alternative splicing of *Eif4a2*, *Rbm7* (Kadota et al., 2020), and *Tau* (Gu et al., 2012)), we identified 1857 total SRSF7-dependent AS events in resting RAW 264.7 MΦs and 1909 SRSF7-dependent events in RAW 264.7 MΦs 4h post-*Salmonella* infection (**Fig. 1C**) ($p<0.05$; >10% PSI). As expected for an SR protein that promotes exon recognition/inclusion, most changes were at the level of exon skipping. Of the 964 genes for which local splicing variation was measured in resting MΦs and the 993 genes in *Salmonella*-infected macrophages, 493 of these genes overlapped (**Fig. 1D**). Notably, only a handful of the detected alternative splicing changes occurred in genes that were also differentially expressed in *Srsf7* knockdown macrophages, suggesting that *Srsf7* impacts steady state RNA levels in a splicing-independent fashion (**Fig. 1E**).

Based on these findings, we hypothesized that SRSF7 mediates distinct alternative splicing events in the two macrophage states. To begin to test this, we prioritized a set of genes with the most significant SRSF7-dependent AS changes (>20% PSI; confidence threshold 0.95) in each condition (resting (UN) and 4h post-*Salmonella* infection (+SAL)) (**Fig. S1A**). Manual annotation of these 36 genes did not reveal significant enrichment for any functional category and none of the top AS events occurred in genes with characterized roles in the MΦ innate immune response (**Fig. S1A**). To visualize and validate SRSF7-dependent AS in resting and *Salmonella*-infected macrophages, we looked at exon 6 skipping in *Dcun1d2* (Ensembl Transcript ID: ENSMUST00000045366.10), a gene associated with Cullin neddylation (Kajigaya et al., 2016). MAJIQ measured significant enrichment of this exon skipping event in both untreated and *Salmonella*-infected *Srsf7* knockdown MΦs (ΔPSI 39.2% in UN and 43.4% in +SAL) (**Fig. 1F-G**). To confirm this event, we performed semi-quantitative RT-PCR, using RNA isolated from SCR, *Srsf7* KD #1 and #2 MΦs, untreated and 4h post-stimulation with lipopolysaccharide (LPS), which activates TLR4 in MΦs in a manner analogous to *Salmonella* infection but provides tighter kinetic

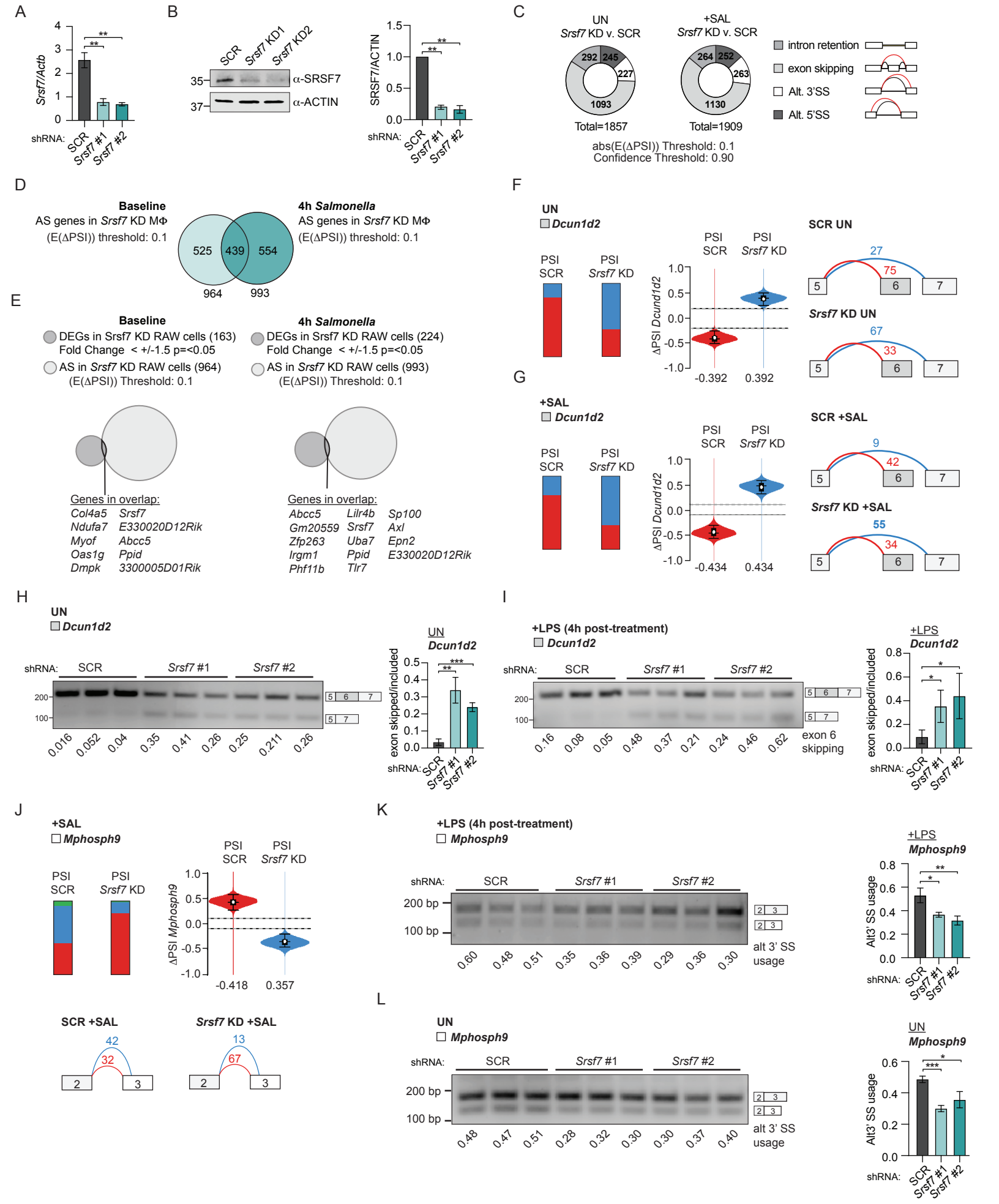
A
Srsf7/Actb
shRNA: SCR Srsf7 #1 Srsf7 #2
B
SCR Srsf7 KD1 Srsf7 KD2
α-SRSF7
α-ACTIN
SRSF7/ACTIN
C
UN
Srsf7 KD v. SCR
+SAL
Srsf7 KD v. SCR
292 245 227 1093
Total=1857
264 252 263 1130
Total=1909
intron retention
exon skipping
Alt. 3'SS
Alt. 5'SS
abs(E(ΔPSI)) Threshold: 0.1
Confidence Threshold: 0.90
D
Baseline
AS genes in Srsf7 KD MΦ
(E(ΔPSI)) threshold: 0.1
525 439 554
964 993
4h Salmonella
AS genes in Srsf7 KD MΦ
(E(ΔPSI)) threshold: 0.1
E
Baseline
DEGs in Srsf7 KD RAW cells (163)
Fold Change < +/-1.5 p=<0.05
AS in Srsf7 KD RAW cells (964)
(E(ΔPSI)) Threshold: 0.1
4h Salmonella
DEGs in Srsf7 KD RAW cells (224)
Fold Change < +/-1.5 p=<0.05
AS in Srsf7 KD RAW cells (993)
(E(ΔPSI)) Threshold: 0.1
Genes in overlap:
Col4a5 Srsf7
Ndufa7 E330020D12Rik
Myof Abcc5
Oas1g Ppid
Dmpk 3300005D01Rik
Genes in overlap:
Abcc5 Lilr4b Sp100
Gm20559 Srsf7 Axl
Zfp263 Uba7 Epn2
Irgm1 Ppid E330020D12Rik
Phf11b Tlr7
F
UN
Dcun1d2
PSI SCR
PSI Srsf7 KD
ΔPSI Dcund1d2
-0.392 0.392
SCR UN
27 75
Srsf7 KD UN
67 33
G
+SAL
Dcun1d2
-0.434 0.434
SCR +SAL
9 42
Srsf7 KD +SAL
55 34
H
UN
Dcun1d2
shRNA: SCR Srsf7 #1 Srsf7 #2
0.016 0.052 0.04 0.35 0.41 0.26 0.25 0.211 0.26
exon skipped/included
I
+LPS (4h post-treatment)
Dcun1d2
0.16 0.08 0.05 0.48 0.37 0.21 0.24 0.46 0.62
exon 6 skipping
J
+SAL
Mphosph9
ΔPSI Mphosph9
-0.418 0.357
SCR +SAL
42 32
Srsf7 KD +SAL
13 67
K
+LPS (4h post-treatment)
Mphosph9
200 bp
100 bp
0.60 0.48 0.51 0.35 0.36 0.39 0.29 0.36 0.30
alt 3' SS usage
Alt3' SS usage
L
UN
Mphosph9
0.48 0.47 0.51 0.28 0.32 0.30 0.30 0.37 0.40

Figure 1

Figure 1: SRSF7 controls alternative splicing in macrophages in an activation-independent fashion

A RT-qPCR of *Srsf7* in *Srsf7* KD RAW MΦs relative to SCR controls. **B.** Immunoblot of SRSF7 in shSCR, sh*Srsf7* #1, sh*Srsf7* #2 RAW 264.7 macrophages. Right, quantification. **C.** Local splicing variations (AS) in *Srsf7* RAW 264.7 cells compared to SCR at baseline (UN; left) and +*Salmonella* Typhimurium (4h) (+SAL; right). ∆PSI > 0.1 confidence threshold set at 0.90. **D.** Venn diagram of genes containing one or more AS event in UN vs. +SAL samples. **E.** Venn diagram of differentially expressed genes (DEGs) vs. alternatively spliced genes (AS) in UN and +SAL samples. **F.** MAJIQ PSI quantification of junctions with SCR (left) and *Srsf7* KD (right) in UN samples. Violin plot of ∆PSI *Dcun1d2* SRSF7-dependent local splicing variation. Splice graph of *Dcun1d2* in SCR (top) and *Srsf7* KD (bottom) generated by MAJIQ/VOILA **G.** As in F but for +SAL samples. **H.** Semi-quantitative PCR of *Dcun1d2* in SCR, *Srsf7* KD #1 and KD #2 RAW 264.7 cells. Each sample in biological triplicate. Right, quantification. **I.** As in H but for *Dcun1d2* +LPS (4h) **J.** As in F but *Mphosph9.* **K.** As in H but *Mphosph9* (+4h LPS). **L.** As in H but *Mphosph9* in UN samples. Data are expressed as a mean of three or more biological replicates with error bars depicting SEM. Statistical significance was determined using two tailed unpaired student's t test. *=p<0.05, **=p<0.01, ***=p<0.001.

A

SRSF7-dependent Untreated (UN)

- Cep295
- Chd9
- Emsy
- Gripap1
- Atp11c
- Hip1
- Knt1
- Miga1
- Odf2l
- Rnf214
- Rsrc1
- Slc11a
- Cd300lf
- Cenpx
- Elk4

>20% PSI

SRSF7-dependent +*Salmonella* (+SAL)

- Dop1a
- Erc1
- Hp1bp3
- Loxl3
- Prr14l
- Sertad2
- Znf496
- Cspp1
- Ncapg2
- Slc25a36
- Brd1
- Clcn4
- Fance
- Lrif1
- Mphosph9

>20% PSI

SRSF7-dependent in both conditions

- Afdn
- Dcun1d2
- Pphln1
- Sapcd2
- Wnk1
- Tuft1

>20% PSI

Functional category
Mitochondria
Chromatin/Transcription
Signaling/Trafficking
Other

Type of AS event
IR
ES
A5SS
A3SS

B

UN
Gripap1

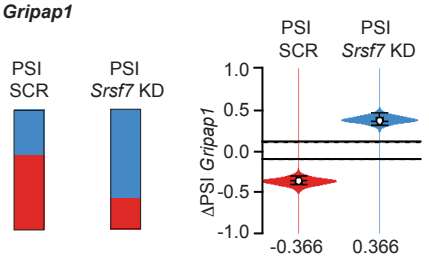

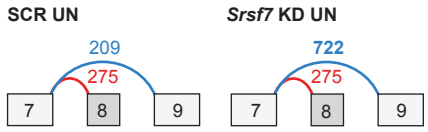

C

UN
Gripap1

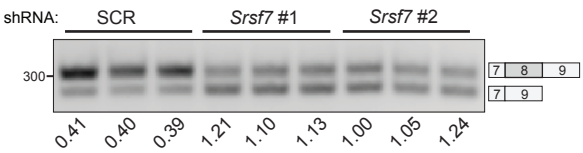

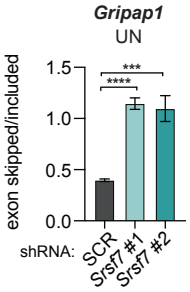

+LPS (4h post-treatment)
Gripap1

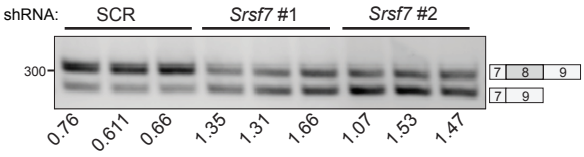

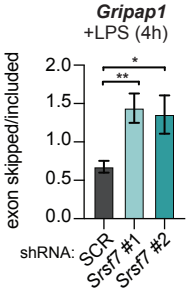

D

+SAL
Dop1a

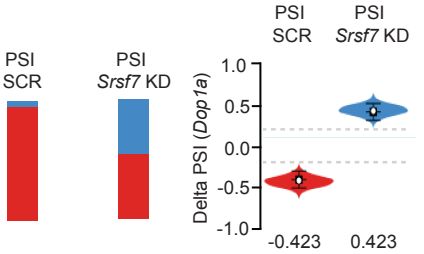

E

+LPS (4h post-treatment)
Dop1a

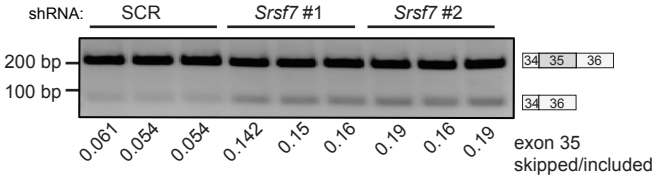

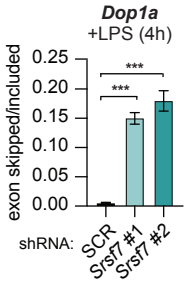

UN
Dop1a

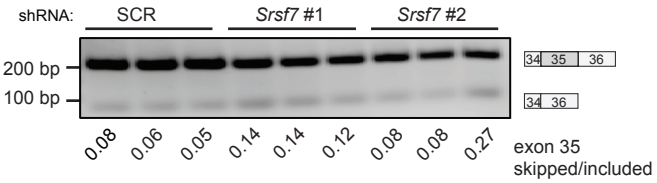

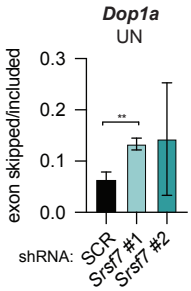

Figure S1: Supplemental data for Figure 1

A. Functional categorization of transcripts differentially spliced in *Srsf7* knockdown RAW 264.7 vs. SCR cells (UN, +SAL, and ∆PSI > 0.2 confidence threshold set at 0.95. **B.** MAJIQ PSI quantification of junctions with SCR (left) and *Srsf7* KD (right). Violin plot of ∆PSI *Gripap1* SRSF7-dependent local splicing variation. Splice graph of *Gripap1* in SCR (bottom left) and *Srsf7* KD (bottom right) generated by MAJIQ/VOILA at baseline. **C.** Semiquantitative PCR of *Gripap1* in SCR, *Srsf7* KD1 and KD2 RAW 264.7 cells, UN (top) and 4h +LPS (bottom). Each sample in biological triplicate. Right, quantification. **D.** MAJIQ PSI quantification of junctions with SCR (left) and *Srsf7* KD (right). Violin plot of ∆PSI *Dop1a* SRSF7-dependent local splicing variation. Splice graph of *Dop1a* in SCR (bottom left) and *Srsf7* KD (bottom right) generated by MAJIQ/VOILA at baseline. **E** Semiquantitative PCR of *Gripap1* in SCR, *Srsf7* KD #1 and KD #2 RAW 264.7 cells, UN (top) and 4h +LPS (bottom). Each sample in biological triplicate. Right, quantification. Data are expressed as a mean of three biological replicates with error bars depicting SEM. Statistical significance was determined using two tailed unpaired student's t test. *=p<0.05, **=p<0.01, ***=p<0.001, ****=p<0.0001.

171 control experimentally. Consistent with our MAJIQ analysis, we measured significantly higher lev-
172 els of *Dcun1d2* exon 6 skipping in *Srsf7* knockdown MΦs in both conditions (**Fig. 1H-I**).
173 We then measured condition-specific SRSF7-dependent splicing events, based on pre-
174 dictions made by the MAJIQ algorithm (**Fig. 1D**). In +SAL samples, MAJIQ quantified SRSF7-
175 dependent alternative 3'SS usage in exon 3 of the *Mphosph9* gene (Ensembl Transcript ID:
176 ENSMUST00000184951.8) that encodes an M-phase phosphoprotein (*Srsf7* knockdown #2
177 (ΔPSI -35.7%) (**Fig. 1J**). RT-PCR confirmed this SRSF7-dependent AS event in LPS-treated MΦs
178 (**Fig. 1K**). Curiously, we measured similar levels of alternative 3'SS usage in untreated *Srsf7*
179 knockdown MΦs (**Fig. 1L**), even though this event was not called by the splicing algorithm.
180 SRSF7-dependent inclusion of exon 8 in *Gripap1* (Ensembl Transcript ID
181 ENSMUST00000065932.14) (**Fig. S1B**), and inclusion of exon 35 in *Dop1a* (Ensembl Transcript
182 ID ENSMUST00000190957.7) (**Fig. S1D)** only met our threshold in UN and +SAL conditions,
183 respectively, but could be detected in both macrophage states by RT-PCR (**Fig. S1C, S1E**).
184 These data argue that SRSF7 mediates the same AS events in resting and activated MΦs. Based
185 on the nature of the genes whose AS relies on SRSF7 and the lack of specificity for events be-
186 tween resting and activated MΦs, we can conclude that SRSF7 is unlikely to dramatically influ-
187 ence the macrophage innate immune transcriptome at the level of splicing.
188
189 **SRSF7 is a positive regulator of type I interferon transcript accumulation in macrophages**
190 In addition to our AS analysis, we also measured differentially expressed genes in *Srsf7* knock-
191 down vs. SCR control RAW MΦs, both in untreated cells and at 4h post-*Salmonella* infection
192 (Wagner et al., 2021). Consistent with our studies of other SR proteins (Wagner et al., 2021;
193 Wagner et al., 2022)), *Srsf7* knockdown impacted expression of many housekeeping genes in
194 resting MΦs, particularly in pathways related to translation regulation (EIF2 signaling and Regu-
195 lation of eIF4 and p70S6K signaling) and phagosome maturation (**Fig. S2A**). Interestingly, in
196 resting MΦs, we also saw enrichment for SRSF7-dependent genes in pathways like "Communi-
197 cation between innate and adaptive immune cells" (**Fig. S2A**), suggesting a dysregulation of in-
198 nate immune genes in *Srsf7* knockdown MΦs even in the absence of an innate stimulus. Enrich-
199 ment for pathways related to innate immunity was also evident in *Salmonella*-infected samples,
200 where *Srsf7* knockdown dysregulated genes in pathways related to "role of pattern recognition
201 receptors in recognition of bacteria and viruses," "interferon signaling," "role of PKR in interferon
202 induction and antiviral response," and "activation of IRF by cytosolic pattern recognition receptors"
203 (**Fig. S2B**). Many of these categories contain genes related to the type I interferon (IFN) response,
204 a ubiquitous antiviral response characterized by expression of *Ifnb1* and interferon stimulated

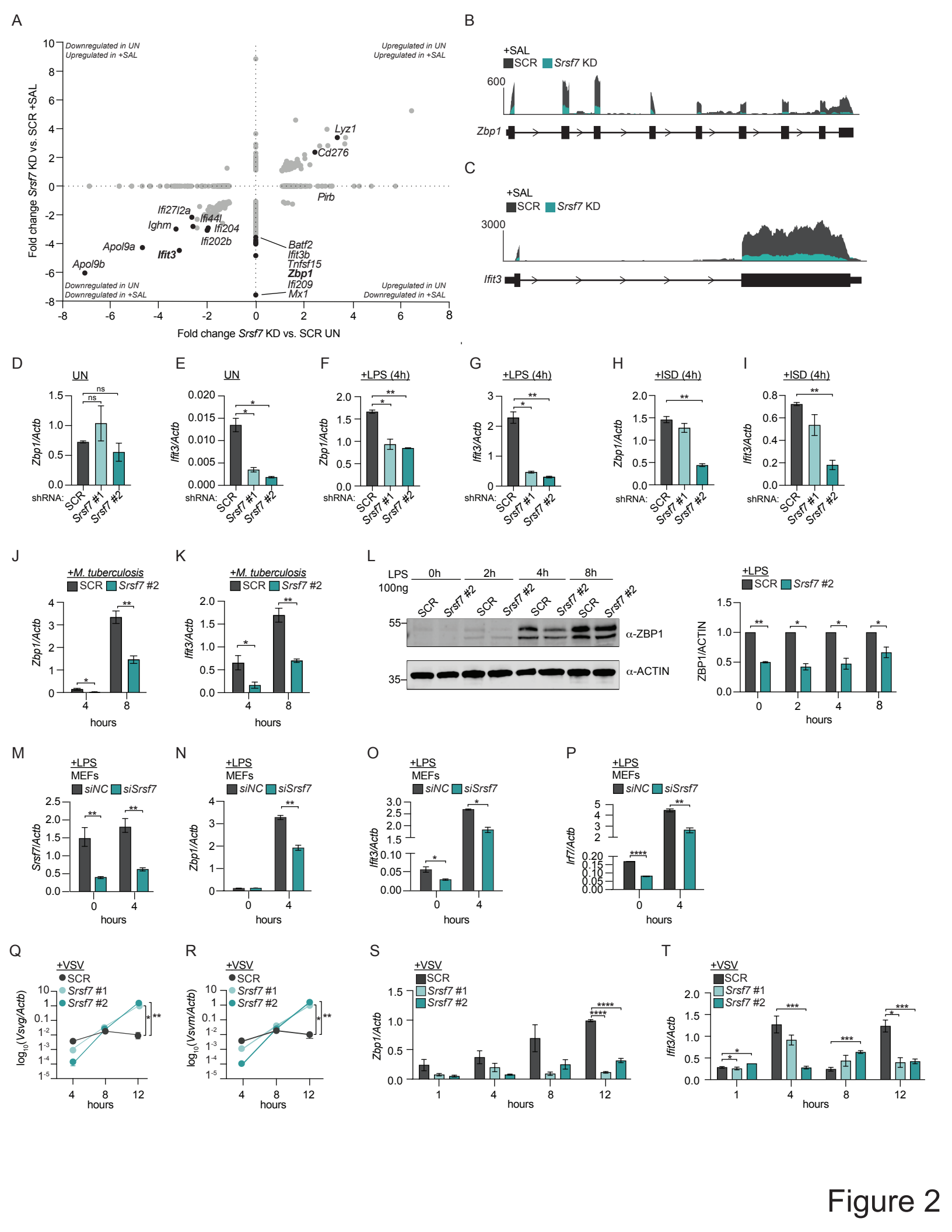
A
Downregulated in UN
Upregulated in +SAL
Upregulated in UN
Upregulated in +SAL
Downregulated in UN
Downregulated in +SAL
Upregulated in UN
Downregulated in +SAL
Fold change Srsf7 KD vs. SCR +SAL
Fold change Srsf7 KD vs. SCR UN
Lyz1
Cd276
Pirb
Ifi27l2a
Ifi44l
Ighm
Ifi204
Ifi202b
Apol9a
Ifit3
Apol9b
Batf2
Ifit3b
Tnfsf15
Zbp1
Ifi209
Mx1
B
+SAL
SCR
Srsf7 KD
600
Zbp1
C
+SAL
SCR
Srsf7 KD
3000
Ifit3
D
UN
Zbp1/Actb
shRNA:
SCR
Srsf7 #1
Srsf7 #2
E
UN
Ifit3/Actb
F
+LPS (4h)
Zbp1/Actb
G
+LPS (4h)
Ifit3/Actb
H
+ISD (4h)
Zbp1/Actb
I
+ISD (4h)
Ifit3/Actb
J
+M. tuberculosis
SCR
Srsf7 #2
Zbp1/Actb
hours
K
+M. tuberculosis
SCR
Srsf7 #2
Ifit3/Actb
hours
L
LPS
100ng
0h
2h
4h
8h
SCR
Srsf7 #2
55
35
α-ZBP1
α-ACTIN
+LPS
SCR
Srsf7 #2
ZBP1/ACTIN
hours
M
+LPS
MEFs
siNC
siSrsf7
Srsf7/Actb
hours
N
+LPS
MEFs
siNC
siSrsf7
Zbp1/Actb
hours
O
+LPS
MEFs
siNC
siSrsf7
Ifit3/Actb
hours
P
+LPS
MEFs
siNC
siSrsf7
Irf7/Actb
hours
Q
+VSV
SCR
Srsf7 #1
Srsf7 #2
log10(Vsvg/Actb)
hours
R
+VSV
SCR
Srsf7 #1
Srsf7 #2
log10(Vsvm/Actb)
hours
S
+VSV
SCR
Srsf7 #1
Srsf7 #2
Zbp1/Actb
hours
T
+VSV
SCR
Srsf7 #1
Srsf7 #2
Ifit3/Actb
hours

Figure 2

Figure 2: SRSF7 promotes type I interferon expression.

A. Scatterplot of genes differentially expressed in *Srsf7* KD RAW MΦs relative to SCR in each of the conditions queried (X axis = UN; Y axis = +SAL). **B.** Integrated Genomics Viewer track of *Zbp1* reads in +SAL samples. SCR (grey) and *Srsf7* KD reads (teal). **C.** As in B but for *Ifit3.* **D.** RT-qPCR of *Zbp1* in SCR and *Srsf7* KD#1 or KD#2 RAW 264.7 MΦs at baseline (UN). **E.** As in D but for *Ifit3.* **F.** RT-qPCR of *Zbp1* in SCR and *Srsf7* KD#1 or KD#2 RAW 264.7 MΦs 4h post stimulation with 100 ng/ml LPS. **G.** As in F but for *Ifit3.* **H.** RT-qPCR of *Zbp1* in SCR and *Srsf7* KD #1 or KD #2 RAW 264.7 MΦs 4h post-transfection with 1 µg/ml ISD. **I.** As in F but for *Ifit3.* **J.** RT-qPCR of *Zbp1* in SCR and *Srsf7* KD #2 RAW 264.7 MΦs 4 or 8h post infection with *M. tuberculosis* (Erdman strain; MOI=5). **K.** As in J but for *Ifit3.* **L.** Immunoblot of ZBP1 protein levels in SCR and *Srsf7* KD #2 cells at baseline, 4, and 8h, post stimulation with 100 ng/ml LPS. Right, quantification. **M.** RT-qPCR of *Srsf7* in primary MEFs at baseline or 4h post stimulation with 100ng LPS. **N.** As in M but for *Zbp1*. **O.** As in M but for *Ifit3*. **P.** As in M but for *Irf7*. **Q.** RT-qPCR of *Vsvg* in SCR, *Srsf7* KD #1, and *Srsf7* KD #2 RAW 264.7 MΦs over a time course (4, 8, 12h) post infection with VSV (MOI=0.1). **R.** As in M but for *Vsvm.* **S.** RT-qPCR of *Zbp1* in SCR, *Srsf7* KD #1, *Srsf7* KD #2 RAW 264.7 MΦs over a time course (1, 4, 8, 12h) post infection with VSV MOI=0.1. **T.** As in S but for *Ifit3.* Data are expressed as a mean of three biological replicates with error bars depicting SEM. Statistical significance was determined using two tailed unpaired student's t test. *=p<0.05, **=p<0.01, ***=p<0.001, ****=p<0.0001.

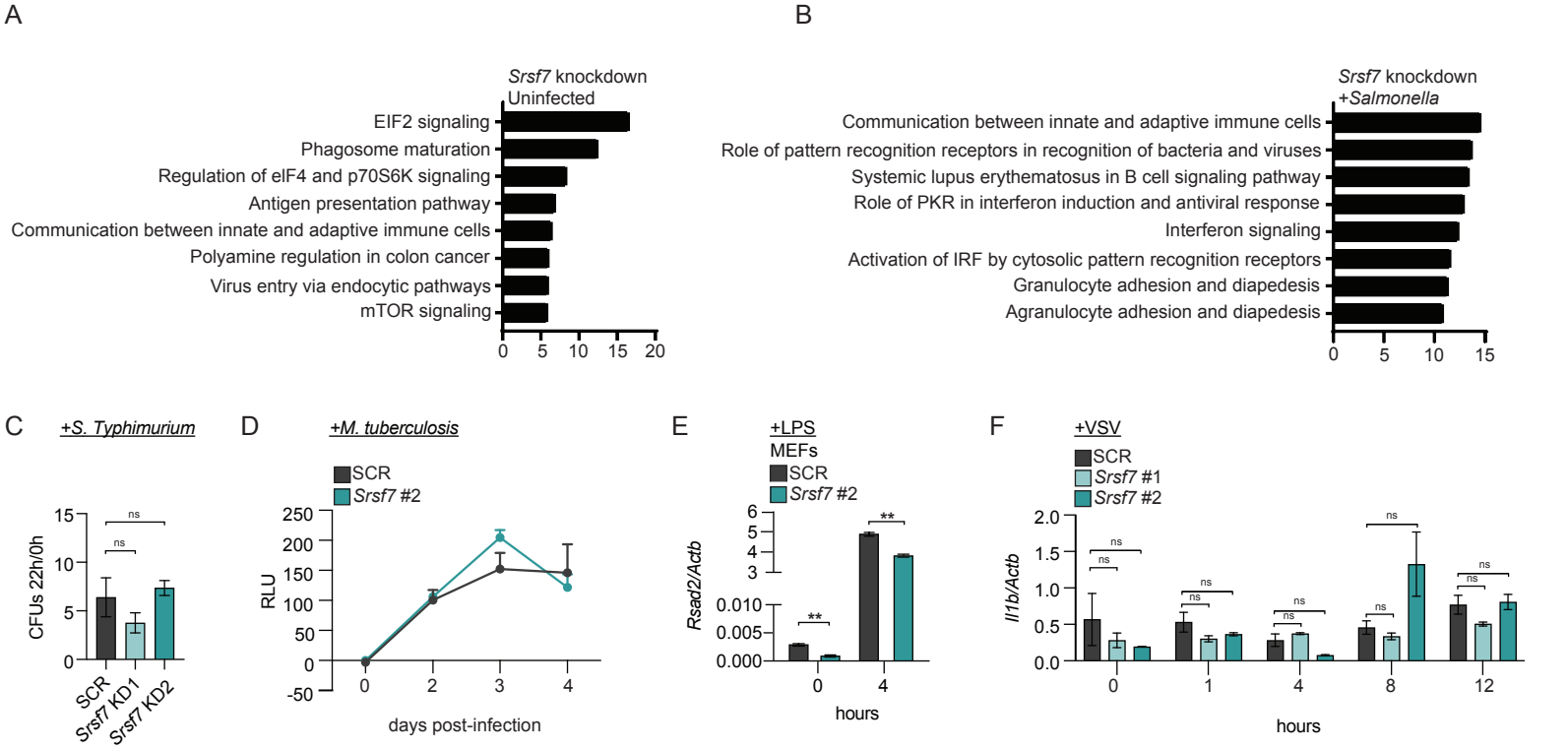
A
Srsf7 knockdown
Uninfected
EIF2 signaling
Phagosome maturation
Regulation of eIF4 and p70S6K signaling
Antigen presentation pathway
Communication between innate and adaptive immune cells
Polyamine regulation in colon cancer
Virus entry via endocytic pathways
mTOR signaling
0 5 10 15 20
B
Srsf7 knockdown
+Salmonella
Communication between innate and adaptive immune cells
Role of pattern recognition receptors in recognition of bacteria and viruses
Systemic lupus erythematosus in B cell signaling pathway
Role of PKR in interferon induction and antiviral response
Interferon signaling
Activation of IRF by cytosolic pattern recognition receptors
Granulocyte adhesion and diapedesis
Agranulocyte adhesion and diapedesis
0 5 10 15
C
+S. Typhimurium
CFUs 22h/0h
ns
ns
SCR
Srsf7 KD1
Srsf7 KD2
D
+M. tuberculosis
SCR
Srsf7 #2
RLU
days post-infection
E
+LPS
MEFs
SCR
Srsf7 #2
Rsad2/Actb
**
**
hours
F
+VSV
SCR
Srsf7 #1
Srsf7 #2
Il1b/Actb
ns
hours

S2

Figure S2: Supplemental data for Figure 2

A. Ingenuity Pathway Analysis (IPA; Qiagen) of pathways enriched for differentially expressed genes in *Srsf7* KD RAW 264.7 MΦs (UN). **B.** As in A for *Srsf7* KD RAW 264.7 MΦs +SAL. **C.** Infection of SCR or *Srsf7* KD RAW 264.7 MΦs with *Salmonella* enterica (MOI=1) in non-SPI-1 inducing conditions. Replication represented as fold 22h over 2h post infection. **D.** Mtb luxBCADE growth in SCR or *Srsf7* KD RAW 264.7 MΦs measured by relative light units (RLUs) over a 4-day time course (MOI=1). **F.** RT-qPCR of *Rsad2* in siRNA *Srsf7*- or siControl-transfected primary MEFs at baseline or 4h post stimulation with 100ng/ml of LPS. **G.** RT-qPCR of *Il1b* in SCR or *Srsf7* KD RAW 264.7 MΦs over a time course of VSV infection. Data are expressed as a mean of three or more biological replicates with error bars depicting SEM. Statistical significance was determined using two tailed unpaired student's t test. *=$p<0.05$, **=$p<0.01$.

genes (ISGs) (Schoggins, 2019; Schoggins and Rice, 2011). In MΦs, the type I IFN response is activated by the transcription factors IRF3 and IRF7 in response to several immune agonists including LPS/*Salmonella* infection, cytosolic dsDNA, and cytosolic dsRNA (21478870 (Honda and Taniguchi, 2006; Jefferies, 2019; Schoggins et al., 2011).

Certain ISGs are maintained in MΦs at low basal levels (Barrat et al., 2019; Gough et al., 2012)). We observed that *Srsf7* knockdown decreased abundance of ISGs like *Apol9a*, *Apol9b*, *Ifit3*, and *Ifi202b*, which are appreciably expressed in resting MΦs (**Fig. 2A**; bottom left quadrant). On the other hand, genes like *Mx1, Zbp1,* and *Ifi209*, which are virtually undetectable in resting cells, only displayed *Srsf7*-dependence in our *Salmonella*-infected samples (**Fig. 2A**; lower y-axis). Visualizing RNA reads from two such ISGs, *Zbp1* and *Ifit3*, on the Integrated Genomics Viewer (Broad Institute), we did not notice any changes in intronic reads in *Srsf7* knockdown versus control cells (**Fig. 2B-C**). This was consistent with our MAJIQ analysis, which did not detect many statistically significant splicing changes in genes annotated as ISGs in *Srsf7* knockdown RAW MΦs (**Fig. 1E)**.

We predicted that failure to phagocytose *Salmonella* or defects in *Salmonella* replication could result in lower ISG expression in *Srsf7* knockdown cells, but enumeration of colony forming units (CFUs) did not reveal any differences in bacterial burdens between SCR and *Srsf7* knockdown RAW MΦs over a 22h infection time-course (**Fig. S2C**). To determine if SRSF7's ability to promote ISG expression was unique to *Salmonella* infection, we measured ISG expression in SCR and *Srsf7* knockdown MΦs at 4h post-treatment with LPS (100 ng/ml), after dsDNA transfection (1 μg ISD), which activates type I IFN gene expression downstream of cGAS, and after treatment with recombinant IFN-β (200 IU, 4h), which activates ISG expression in MΦs by binding to IFNAR and engaging JAK/STAT cascades. In all cases, loss of *Srsf7* led to impaired activation of *Zbp1* and *Ifit3* expression (**Fig. 2D-I**). We also measured lower ISG expression in *Srsf7* knockdown MΦs during infection with the intracellular bacterial pathogen, *Mycobacterium tuberculosis* (MOI = 5) (**Fig. 2J-K**), which elicits *Ifnb1* and ISG expression via the cGAS/STING pathway (Watson et al., 2015). Again, this defect in ISG expression was independent of bacterial internalization/replication (**Fig. S2D**). Importantly, over an 8h time-course of LPS-treatment, lower *Zbp1* transcript levels correlated with lower protein accumulation (**Fig. 2L**), suggesting that failure to fully upregulate ISG expression in *Srsf7* knockdown MΦs is likely to functionally impact the innate immune response to infection. This phenotype was not unique to RAW MΦs, as loss of SRSF7 in primary mouse embryonic fibroblasts (MEFs) via siRNA transfection (alongside siNC transfected controls) (**Fig. 2M**) also resulted in low basal ISG expression and a failure to fully induce ISGs upon LPS stimulation (**Fig. 2N-P and S2E)**

239 To test whether SRSF7 is a *bona fide* player in activating antimicrobial immunity in MΦs,
240 we infected SCR and *Srsf7* knockdown MΦs with vesicular stomatitis virus (VSV), a negative-
241 strand RNA virus that stimulates type I IFN responses via TLR3 and RIG-I and is extremely sen-
242 sitive to type I IFN expression (Gao et al., 2021; Wagner et al., 2021)). While genes like *Ifnb1* and
243 ISGs are robustly induced by bacterial pathogens (e.g. *Salmonella* and *M. tuberculosis*), they are
244 most studied during viral infection, where they function to inhibit different steps of the viral life
245 cycle (Schoggins, 2019). We measured a dramatic increase in VSV replication in *Srsf7* knock-
246 down MΦs, measured by RT-qPCR of two VSV genes, *Vsvg* and *Vsvm* (**Fig. 2Q-R**) that was
247 concomitant with depressed ISG transcript induction over a 12-hour time course of VSV infection
248 (MOI = 0.1) (**Fig. 2S-T**). We did not detect SRSF7-dependent differences in *Il1b* expression in
249 response to VSV infection, arguing against a role for SRSF7 in controlling innate gene expression
250 downstream of NFκB (**Fig. S2F**). Together, these data identify SRSF7 as a positive regulator of
251 the type I IFN response in MΦs and suggest that the mechanism of SRSF7-dependent ISG ex-
252 pression is shared by several pathogen sensing cascades (i.e. occurs at one or more nodes where
253 the TLR4, cGAS, and RIG-I cascades converge).
254
255 **SRSF7 drives ISG expression without interfering with innate immune signaling.**
256 Given that loss of SRSF7 results in a failure to fully induce many ISGs, we hypothesized
257 that SRSF7 may act directly on one or more critical innate signaling proteins or transcription fac-
258 tors. To pinpoint where in the type I IFN signaling response SRSF7 acts, we treated *Srsf7*
259 knockdown or SCR RAW MΦs with LPS (100 ng/ml) and measured secretion of type I interferon
260 (IFN-β/α) over a 6h time-course via a luciferase ISRE reporter cell line (Hoffpauir et al., 2020;
261 Wagner et al., 2022)). *Srsf7* knockdown MΦs produced significantly less IFN-β/α compared to
262 SCR controls at all time points measured (**Fig. 3A**). We next asked if impaired ISG expression
263 in *Srsf7* knockdown MΦs could be rescued if *Srsf7* knockdown and SCR control cells received
264 equal amounts of recombinant IFN-β, a potent type I interferon driver. We found that even in the
265 presence of high amounts of IFN-β, *Srsf7* knockdown MΦs fail to express ISGs like *Ifi202b* and
266 *Zbp1* to the same level as SCR controls, at both the transcript (**Fig. 3B-C**) and protein level
267 (**Fig. 3D**). These results suggest that loss of SRSF7 impacts some aspect of the type I IFN re-
268 sponse that is engaged upstream and downstream of IFNAR and that loss of IFN-β production
269 is not the sole driver of ISG defects in *Srsf7* knockdown MΦs.
270 We then asked whether altered signaling downstream of IFNAR could explain defective
271 ISG expression in *Srsf7* knockdown RAW MΦs. We treated *Srsf7* knockdown and SCR RAW
272 MΦs with LPS and measured phosphorylation of the transcription factor IRF3 (activated

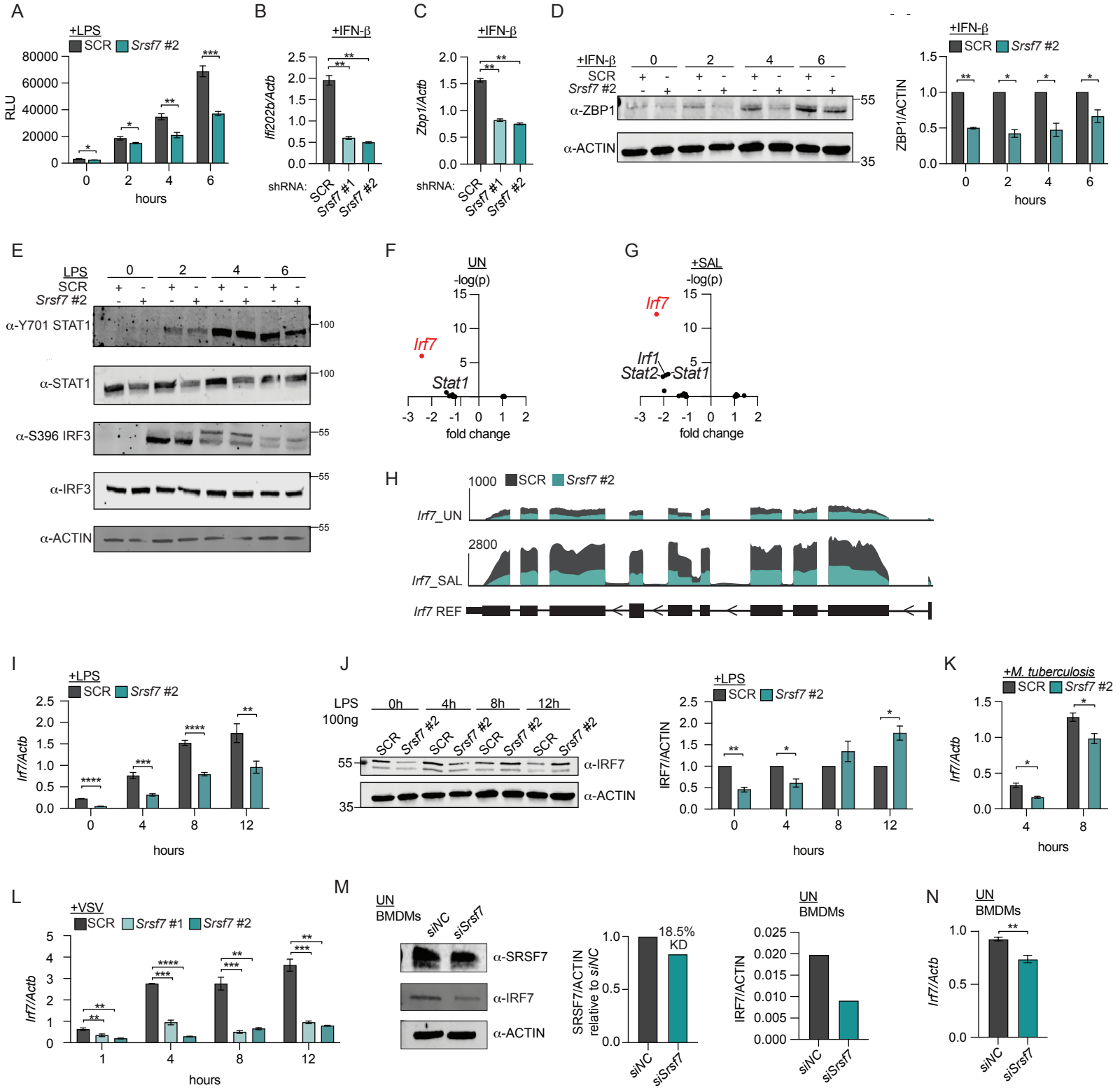
A
+LPS
SCR
Srsf7 #2
RLU
hours
B
+IFN-β
Ifi202b/Actb
shRNA:
SCR
Srsf7 #1
Srsf7 #2
C
+IFN-β
Zbp1/Actb
shRNA:
SCR
Srsf7 #1
Srsf7 #2
D
+IFN-β
SCR
Srsf7 #2
α-ZBP1
α-ACTIN
+IFN-β
SCR
Srsf7 #2
ZBP1/ACTIN
hours
E
LPS
SCR
Srsf7 #2
α-Y701 STAT1
α-STAT1
α-S396 IRF3
α-IRF3
α-ACTIN
F
UN
-log(p)
Irf7
Stat1
fold change
G
+SAL
-log(p)
Irf7
Irf1
Stat2
Stat1
fold change
H
SCR
Srsf7 #2
Irf7_UN
Irf7_SAL
Irf7 REF
I
+LPS
SCR
Srsf7 #2
Irf7/Actb
hours
J
LPS
100ng
0h
4h
8h
12h
SCR
Srsf7 #2
α-IRF7
α-ACTIN
+LPS
SCR
Srsf7 #2
IRF7/ACTIN
hours
K
+M. tuberculosis
SCR
Srsf7 #2
Irf7/Actb
hours
L
+VSV
SCR
Srsf7 #1
Srsf7 #2
Irf7/Actb
hours
M
UN
BMDMs
siNC
siSrsf7
α-SRSF7
α-IRF7
α-ACTIN
SRSF7/ACTIN relative to siNC
18.5% KD
siNC
siSrsf7
UN
BMDMs
IRF7/ACTIN
siNC
siSrsf7
N
UN
BMDMs
Irf7/Actb
siNC
siSrsf7

Figure 3

Figure 3: SRSF7 is required for IRF7 accumulation in macrophages

A. Secreted IFNα/β in SCR and *Srsf7* KD RAW 264.7 MΦs, as a measure of luciferase expressed by ISRE reporter cells. **B.** RT-qPCR of *Ifi202b* in SCR and *Srsf7* KD RAW 264.7 MΦs 4h post stimulation with 200 IU IFN-β. **C.** As in B for *Zbp1.* **D.** Immunoblot of ZBP1 and ACTIN over a time course of IFN-β (200 IU) treatment in SCR and *Srsf7* KD RAW 264.7 MΦs. Quantification, right. **E.** Immunoblot of Y701 STAT1, STAT1, S396 IRF3, IRF3, and ACTIN in SCR and *Srsf7* KD RAW 264.7 MΦs over a time course of LPS treatment (100ng/ml). **F.** Differential expression of transcription factor genes in untreated *Srsf7* knockdown vs. SCR RAW 264.7 MΦs as fold change and -log(pvalue). **G.** As in F but for +SAL samples. **H.** Integrated Genomics Viewer track of *Irf7* reads in +SAL samples. SCR (grey) and *Srsf7* KD reads (teal). **I.** RT-qPCR of *Irf7* over a time course of LPS stimulation (100ng/ml) in SCR and *Srsf7* KD RAW 264.7 MΦs. **J.** Immunoblot of IRF7 and ACTIN protein levels over a time course of LPS stimulation (100ng/ml) in SCR and *Srsf7* KD RAW 264.7 MΦs. Quantification, right. **K.** RT-qPCR of *Irf7* over a time course of Mtb infection (Erdman strain; MOI=5) in SCR and *Srsf7* KD RAW 264.7 MΦs. **L.** RT-qPCR of *Irf7* over a time course of VSV infection (MOI=0.1) in SCR or *Srsf7* KD RAW 264.7 MΦs. **M.** Immunoblot of SRSF7, IRF7, and ACTIN in siControl- or si*Srsf7*-transfected BMDMs at baseline. Quantifications, right. **N.** RT-qPCR of *Irf7* in siControl or si*Srsf7* BMDMs at baseline. Data expressed as a mean of three biological replicates with error bars depicting SEM. Statistical significance was determined using two tailed unpaired student's t test. *=p<0.05, **=p<0.01, ***=p<0.001, ****=p<0.0001.

A

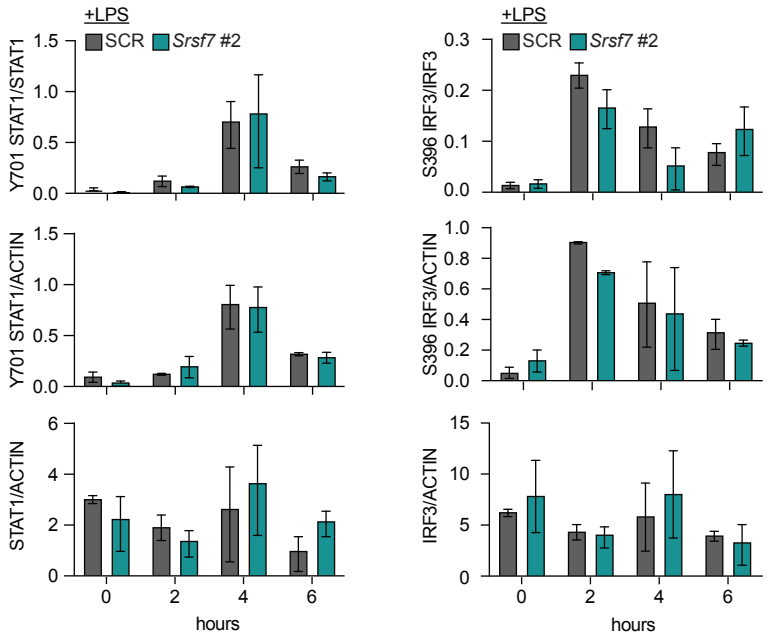
+LPS
SCR
Srsf7 #2
Y701 STAT1/STAT1
Y701 STAT1/ACTIN
STAT1/ACTIN
S396 IRF3/IRF3
S396 IRF3/ACTIN
IRF3/ACTIN
hours

B

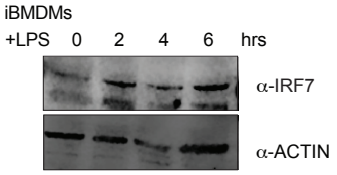
iBMDMs
+LPS 0 2 4 6 hrs
α-IRF7
α-ACTIN

C

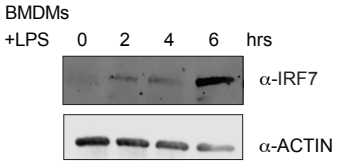
BMDMs
+LPS 0 2 4 6 hrs
α-IRF7
α-ACTIN

Figure S3: Supplemental data for Figure 3

A. Quantification of Figure 3E. n=2 **B.** Immunoblot of IRF7 and ACTIN protein levels over a time course of LPS stimulation (100ng/ml) in WT BMDMs. **C.** As in B but in WT iBMDMs. Data are expressed as a mean of three biological replicates with error bars depicting SEM. Statistical significance was determined using two tailed unpaired student's t test.

273 downstream of TLR4-TRIF signaling) and STAT1 (activated downstream of IFNAR) over a 6h
274 time course. We did not measure significant changes in phosphorylation of IRF3 at S396 or
275 phosphorylation of STAT1 at Y701 (**Fig. 3E**; quantification in **Fig. S3A**) effectively ruling out de-
276 fective signal transduction as the culprit for dampened ISG expression in *Srsf7* knockdown
277 MΦs.
278 Next, we entertained the possibility that SRSF7 is required for the expression of one or
279 more transcription factors needed to activate the type I IFN response downstream of pattern
280 recognition receptor engagement. To test this, we generated a list of transcription factors asso-
281 ciated with macrophage innate immune gene expression in the STAT, IRF, and NFκB families,
282 and turned back to our RNA-seq data to see how expression of each factor was impacted by
283 loss of SRSF7. While expression of most TFs was unaffected, we observed a significant defect
284 in *Irf7* expression in *Srsf7* knockdown RAW MΦs compared to SCR controls at both baseline
285 and after *Salmonella* infection (**Fig. 3F-G**). Visualization of *Irf7* gene expression data on the IGV
286 highlights fewer *Irf7* exonic reads in *Srsf7* knockdown (teal) compared to SCR (grey) RAW MΦs
287 in both conditions (**Fig. 3H**). We did not detect an increase in intron reads in *Srsf7* knockdown
288 MΦs nor did our MAJIQ analysis identify SRSF7-dependent *Irf7* alternative splicing events (**Fig.
289 1D**), arguing against a role for SRSF7 in regulating *Irf7* transcript abundance via splicing.
290 Initially discovered in the context of Epstein Barr virus, IRF7 (interferon regulatory factor
291 7) acts as both a master regulator of antiviral type I IFN responses and an ISG (Honda et al.,
292 2005). Basal amounts of IRF7 vary between immune cell types. Dendritic cells are heavily reli-
293 ant upon IRF7 at baseline and several recent reports identify IRF7 as important for priming bone
294 marrow derived macrophages (BMDMs) downstream of LPS (Fitzgerald et al., 2003; Gu et al.,
295 2022; Jefferies, 2019; Sin et al., 2020). We can readily measure IRF7 transcript and protein in
296 resting WT RAW MΦs (**Fig. 3I-J**) and in WT immortalized BMDMs (**Fig. S3B**). IRF7 protein lev-
297 els are low in WT resting BMDMs but are upregulated in response to LPS (**Fig. S3C**).
298 To better appreciate the kinetics of SRSF7 control of *Irf7* expression, we treated *Srsf7*
299 knockdown and SCR control RAW MΦs with LPS and measured *Irf7* transcript and protein over
300 a 12h time course. We measured significantly lower levels of *Irf7* mRNA in *Srsf7* knockdown
301 RAW MΦs at every time-point queried (**Fig. 3I**). IRF7 protein levels were lower in *Srsf7* knock-
302 down RAW MΦs at 0 and 4h but appeared to rebound at later time points (8 and 12h post-LPS)
303 (**Fig. 3J**), consistent with previous reports of IRF7 stabilization during the innate response to in-
304 fection (Sin et al., 2020). We also measured significantly less *Irf7* transcript in *Srsf7* knockdown
305 RAW MΦs in response to *M. tuberculosis* (**Fig. 3K**) and VSV infection (**Fig. 3L**). Although we
306 were only able to achieve modest knockdown of SRSF7 in BMDMs transfected with an siRNA

307 directed against *Srsf7* (alongside a non-targeting control; siNC) (**Fig. 3M**), we can detect less
308 IRF7 protein (**Fig. 3M**) and transcript (**Fig. 3N**) in these primary cells as well. Together, these
309 data demonstrate a previously unappreciated role for SRSF7 in controlling *Irf7* transcript and
310 protein levels in primary macrophages and in the RAW MΦ cell line.
311
312 **IRF7 controls basal and induced expression of ISGs in RAW MΦs**
313 Our findings argue that loss of ISG expression in *Srsf7* knockdown cells stems primarily
314 from loss of IRF7. However, as most literature points to a role for IRF7 in activated immune
315 cells, we were initially cautious to attribute basal ISG phenotypes in *Srsf7* knockdown MΦs to
316 IRF7. To better understand how IRF7 controls type I IFN responses in resting and activated
317 RAW MΦs, we generated *Irf7* KO RAW MΦs using CRISPR-Cas9 editing. *Irf7*-specific guides
318 were designed to target *Irf7* exon 3 alongside a GFP-specific gRNA as a negative control. Two
319 clonally expanded *Irf7* KO cell lines and a GFP gRNA control cell line were selected and loss of
320 IRF7 protein was confirmed by western blot (**Fig. 4A**). Total RNA from untreated *Irf7* KO #1 and
321 control cell lines as well as from cells stimulated with LPS for 4h (100ng/ml) were sent for RNA-
322 seq analysis (150bp paired end reads; Illumina NovaSeq S4, ~80,000,000 reads per sample un-
323 treated and ~20,000,000 reads per sample +4h LPS). We measured differential expression of
324 896 transcripts (fold-change < -1.5; $p<0.05$) in *Irf7* KO vs. control cells at baseline and 1575
325 genes were differentially expressed in *Irf7* KO MΦs at 4h post-LPS treatment (**Fig. 4B**). Pathway
326 analysis (BioPlanet Pathway Enrichment Analysis, NCATS (Huang et al., 2019) identified inter-
327 feron-related pathways enriched for differentially expressed genes in *Irf7* KO cells at baseline
328 and at 4h post-LPS treatment (**Fig. 4C**). Cataloging these lists of genes, we identified >30 ISGs
329 whose expression was impacted by loss of IRF7 in resting RAW MΦs (**Fig. 4D**), and confirmed
330 significant downregulation of *Ifit3b*, *Zbp1*, and *Ifnb1* in untreated *Irf7* KOs compared to control
331 cells by RT-qPCR (**Fig. 4E**). Visualization of reads for select ISGs on the IGV showed lower lev-
332 els of exonic reads in *Irf7* KO RAW MΦs (purple vs. grey) (**Fig. 4F**). We also measured impaired
333 ISG induction in *Irf7* KO RAW MΦs after LPS treatment, but curiously, while the overall number
334 of genes impacted was higher after LPS treatment, the degree to which their expression was
335 impacted by loss of IRF7, compared to GFP gRNA controls, was less (**Fig. S4B**). We predict
336 this is due to activation of IRF3 that can compensate for loss of IRF7 after stimulation. Im-
337 portantly, we found that differentially expressed ISGs were shared between *Srsf7* KD and *Irf7*
338 KO cells: most of the downregulated ISGs in *Srsf7* knockdown cells are also downregulated in
339 *Irf7* KO MΦs (**Fig. 4G**). Any lack of overlap between these lists likely stems from the fact that
340 complete ablation of IRF7 and a 2-3-fold downregulation of IRF7 in *Srsf7* knockdown cells

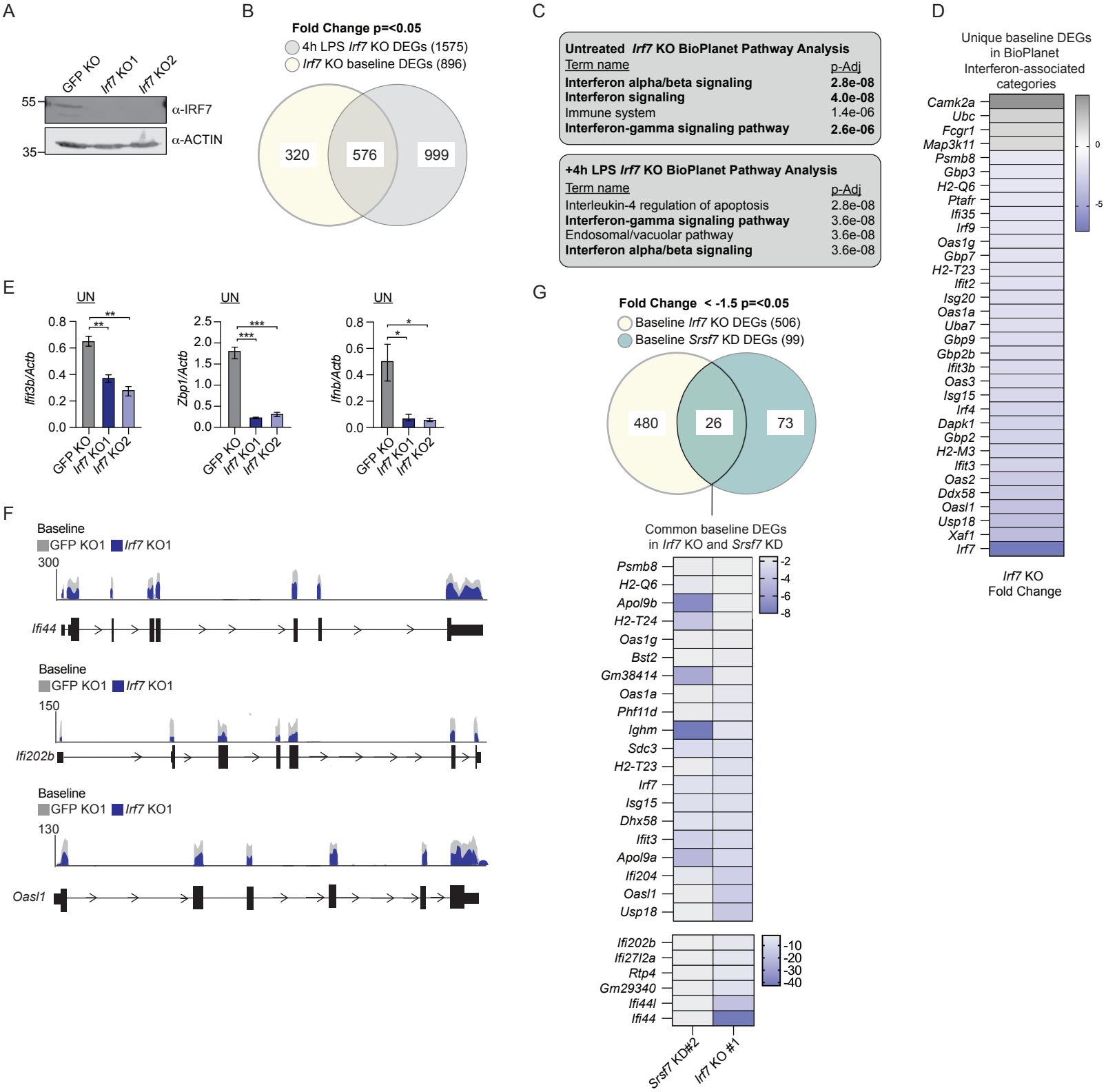
A
GFP KO
Irf7 KO1
Irf7 KO2
55
35
α-IRF7
α-ACTIN
B
Fold Change p=<0.05
4h LPS Irf7 KO DEGs (1575)
Irf7 KO baseline DEGs (896)
320
576
999
C
Untreated Irf7 KO BioPlanet Pathway Analysis
Term name p-Adj
Interferon alpha/beta signaling 2.8e-08
Interferon signaling 4.0e-08
Immune system 1.4e-06
Interferon-gamma signaling pathway 2.6e-06
+4h LPS Irf7 KO BioPlanet Pathway Analysis
Term name p-Adj
Interleukin-4 regulation of apoptosis 2.8e-08
Interferon-gamma signaling pathway 3.6e-08
Endosomal/vacuolar pathway 3.6e-08
Interferon alpha/beta signaling 3.6e-08
D
Unique baseline DEGs in BioPlanet Interferon-associated categories
Camk2a
Ubc
Fcgr1
Map3k11
Psmb8
Gbp3
H2-Q6
Ptafr
Ifi35
Irf9
Oas1g
Gbp7
H2-T23
Ifit2
Isg20
Oas1a
Uba7
Gbp9
Gbp2b
Ifit3b
Oas3
Isg15
Irf4
Dapk1
Gbp2
H2-M3
Ifit3
Oas2
Ddx58
Oasl1
Usp18
Xaf1
Irf7
0
-5
Irf7 KO Fold Change
E
UN
Ifit3b/Actb
Zbp1/Actb
Ifnb/Actb
GFP KO
Irf7 KO1
Irf7 KO2
F
Baseline
GFP KO1
Irf7 KO1
Ifi44
Ifi202b
Oasl1
G
Fold Change < -1.5 p=<0.05
Baseline Irf7 KO DEGs (506)
Baseline Srsf7 KD DEGs (99)
480
26
73
Common baseline DEGs in Irf7 KO and Srsf7 KD
Psmb8
H2-Q6
Apol9b
H2-T24
Oas1g
Bst2
Gm38414
Oas1a
Phf11d
Ighm
Sdc3
H2-T23
Irf7
Isg15
Dhx58
Ifit3
Apol9a
Ifi204
Oasl1
Usp18
Ifi202b
Ifi27l2a
Rtp4
Gm29340
Ifi44l
Ifi44
Srsf7 KD#2
Irf7 KO #1

Figure 4

Figure 4: RAW 264.7 macrophage cell lines are reliant on IRF7 for basal ISG expression
A. Immunoblot of IRF7 protein levels in GFP gRNA, *Irf7* KO1 and *Irf7* KO2 RAW 264.7 MΦs at baseline. ACTIN used as loading control. **B.** Venn diagram depicting differential gene expression of *Irf7* KO1 at baseline vs. 4h +LPS (100ng/ml). Cut off: fold change < -1.5 and p-value=<0.05. **C.** Top: BioPlanet Pathway Analysis of untreated *Irf7* KO gene expression. Bottom: BioPlanet Pathway Analysis of 4h +LPS *Irf7* KO gene expression. **D.** Heatmap depicting *Irf7* KO baseline gene expression from BioPlanet pathway analysis categories: “Interferon alpha/beta signaling,” ”Interferon signaling,” and “Interferon-gamma signaling pathway.” Duplicate terms removed. **E.** RT-qPCR of *Ifit3, Zbp1,* or *Ifnb1* at baseline in *Irf7* KO vs. GFP gRNA control cells. **F.** Integrated Genomics Viewer track of *Ifi44, Ifi202b, and Oasl1* reads in baseline (UN) samples in GFP gRNA (light grey) or *Irf7* KO (dark blue). **G.** Top: Venn diagram depicting DEGs in *Irf7* KO1 (compared to GFP gRNA) and *Srsf7* KD (compared to SCR) RAW 264.7 MΦs at baseline. Bottom: Heatmap of 26 genes in common between *Irf7* KO1 and *Srsf7* KD at baseline. Data are expressed as a mean of three biological replicates with error bars depicting SEM. Statistical significance was determined using two tailed unpaired student’s t test. *=p<0.05, **=p<0.01, ***=p<0.001.

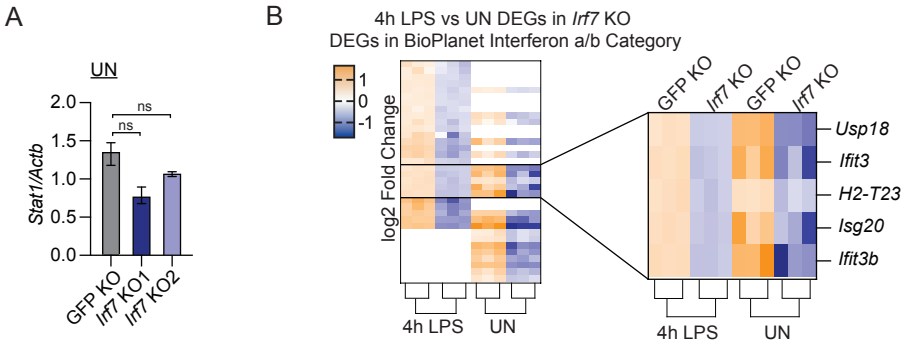
A
UN
Stat1/Actb
2.0
1.5
1.0
0.5
0.0
ns
ns
GFP KO
Irf7 KO1
Irf7 KO2
B
4h LPS vs UN DEGs in Irf7 KO
DEGs in BioPlanet Interferon a/b Category
1
0
-1
log2 Fold Change
4h LPS
UN
GFP KO
Irf7 KO
GFP KO
Irf7 KO
Usp18
Ifit3
H2-T23
Isg20
Ifit3b
4h LPS
UN

Figure S4: Supplemental data for Figure 4

A. RT-qPCR of *Stat1* at baseline (UN) in *Irf7* KO cells. **B.** Heatmap depicting BioPlanet Analysis of genes in the n “interferon a/b signaling” category at baseline or 4h post stimulation with LPS in GFP gRNA or *Irf7* KO RAW 264.7 cells.

341 differentially impact ISG expression in MΦs. Together, these data provide strong evidence for a
342 role for IRF7 in maintaining basal levels of type I IFNs and ISGs in MΦs.
343
344 **SRSF7 is sufficient for IRF7 and ISG expression**
345 Together, our data support a model wherein SRSF7 directly activates *Irf7* transcription. If this
346 were the case, then overexpression of SRSF7 should be sufficient to drive *Irf7* expression. To
347 test this model, we generated doxycycline-inducible MΦs cell lines that express either 3xFLAG-
348 SRSF7 or 3xFLAG-GFP negative control after addition of doxycycline. To ensure comparable
349 levels of 3xFLAG-GFP and 3xFLAG-SRSF7 protein expression, we tested and optimized treat-
350 ment times, deciding on 2h +DOX for GFP and 22h +DOX for SRSF7 (**Fig. 5A**). We found that
351 expression of SRSF7 alone was sufficient to increase the abundance of *Irf7* transcript (**Fig. 5B**)
352 and IRF7 protein levels (**Fig. 5C**) in otherwise unstimulated RAW MΦs. We also measured in-
353 creased expression of ISGs like *Ifit3* in 3xFLAG-SRSF7 MΦs compared to GFP controls (**Fig.**
354 **5D**). To ensure that different lengths of doxycycline treatment was not contributing to our pheno-
355 type, we also measured ISG expression in MΦs stably expressing 3xFLAG-SRSF7 or 3xFLAG-
356 GFP. We found that stable overexpression of 3xFLAG-SRSF7 was also sufficient to drive ISG
357 expression in resting MΦs (**Fig. 5E-G**). The impact of SRSF7 overexpression on *Irf7* following
358 LPS stimulation was less pronounced. We detected increased *Irf7* transcript expression in
359 3xFLAG-SRSF7 expressing cells at 6h post LPS, but this did not correspond to differences in
360 IRF7 protein accumulation (**Fig. S5A,B)**. Given how strong an inducer LPS is of the type I IFN
361 response, it follows that SRSF7 overexpression may not further induce *Irf7* expression on top of
362 these already high levels. We did, however, measure a dramatic increase in *Irf7* and *Ifit3* tran-
363 script levels in 3xFLAG-SRSF7-expressing stable cells upon infection with *M. tuberculosis* (**Fig.**
364 **5H-I**), suggesting that the nature of the stimulus may impact how SRSF7 controls IRF7 and ISG
365 expression. Because expression of type I IFN genes has been associated with cell-intrinsic anti-
366 bacterial control mechanisms and cell death pathways that impact bacterial spread (Patrick et
367 al., 2016), we also asked whether overexpression of SRSF7 affected Mtb replication. Briefly, we
368 infected cells with Mtb luxBCADE and followed bacterial replication as a measure of relative
369 light units (as in (Bell et al., 2021; Wagner et al., 2022)). Remarkably, we measured a significant
370 increase in Mtb RLUs at Day 3 post-infection (**Fig. 5J**) suggesting that SRSF7 expression may
371 help control Mtb replication and/or spread. Together, these data suggest a direct role for the
372 RNA binding protein SRSF7 in promoting expression of *Irf7*.
373
374 **SRSF7 promotes STAT1 association and promoter clearance at the *Irf7* promoter**

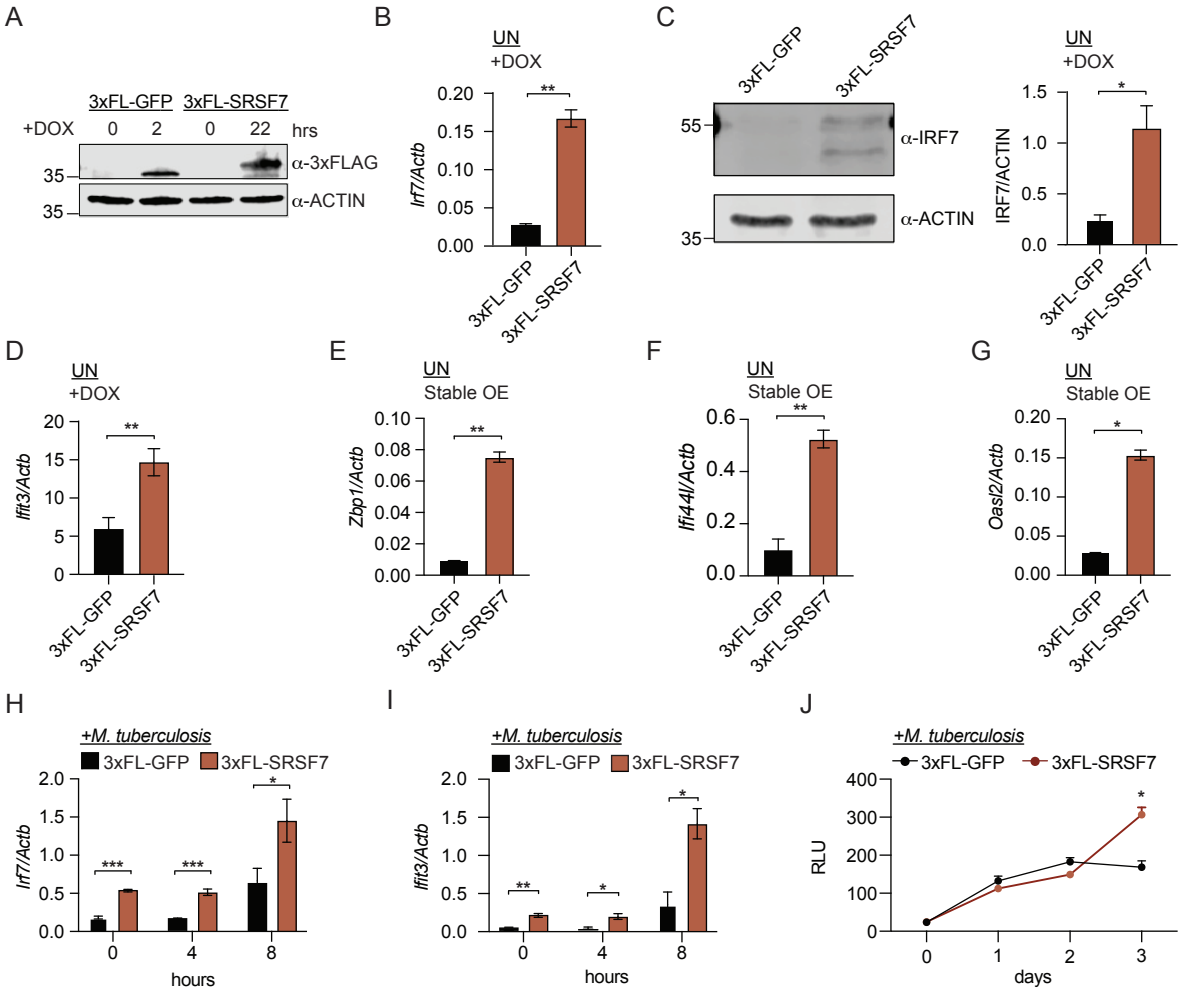
A
3xFL-GFP 3xFL-SRSF7
+DOX 0 2 0 22 hrs
35
α-3xFLAG
35
α-ACTIN
B
UN
+DOX
Irf7/Actb
0.20
0.15
0.10
0.05
0.00
**
3xFL-GFP
3xFL-SRSF7
C
3xFL-GFP
3xFL-SRSF7
55
α-IRF7
35
α-ACTIN
UN
+DOX
IRF7/ACTIN
1.5
1.0
0.5
0.0
*
3xFL-GFP
3xFL-SRSF7
D
UN
+DOX
Ifit3/Actb
20
15
10
5
0
**
3xFL-GFP
3xFL-SRSF7
E
UN
Stable OE
Zbp1/Actb
0.10
0.08
0.06
0.04
0.02
0.00
**
3xFL-GFP
3xFL-SRSF7
F
UN
Stable OE
Ifi44l/Actb
0.6
0.4
0.2
0.0
**
3xFL-GFP
3xFL-SRSF7
G
UN
Stable OE
Oasl2/Actb
0.20
0.15
0.10
0.05
0.00
*
3xFL-GFP
3xFL-SRSF7
H
+M. tuberculosis
3xFL-GFP 3xFL-SRSF7
Irf7/Actb
2.0
1.5
1.0
0.5
0.0
***
***
*
0
4
8
hours
I
+M. tuberculosis
3xFL-GFP 3xFL-SRSF7
Ifit3/Actb
2.0
1.5
1.0
0.5
0.0
**
*
*
0
4
8
hours
J
+M. tuberculosis
3xFL-GFP 3xFL-SRSF7
RLU
400
300
200
100
0
*
0
1
2
3
days

Figure 5

Figure 5: Overexpression of 3xFL-SRSF7 drives basal ISG expression and accumulation of IRF7

A. Immunoblot of 3xFLAG-GFP or 3xFLAG-SRSF7 tetracycline inducible RAW 264.7 MΦs treated with doxycycline (DOX) (1 µg/ml). 3xFLAG-GFP MΦs received DOX for 2h and 3xFLAG-SRSF7 MΦs received DOX for 22h. ACTIN shown as loading control. **B.** RT-qPCR of *Irf7* in 3xFLAG-GFP (2h DOX treatment) or 3xFLAG-SRSF7 (22h DOX treatment) inducible RAW 264.7 cells at baseline. **C.** Immunoblot of IRF7 in 3xFLAG-GFP (2h DOX treatment) or 3xFLAG-SRSF7 (22h dox treatment) inducible RAW 264.7 MΦs at baseline (quantification right). **D.** As in B but for *Ifit3.* **E.** RT-qPCR of *Zbp1* in 3xFLAG-GFP or 3xFLAG-SRSF7 stable overexpression RAW 264.7 MΦs. **F.** As in E but for *Ifi44l* **G.** As in E but for *Oasl2.* **H.** RT-qPCR of *Irf7* over a time course of infection with Mtb (Erdman; MOI=5). **I.** As in H but for *Ifit3* **J.** Mtb luxBCADE replication in 3xFLAG-GFP (2h pretreatment with 1 µg/ml doxycycline) or 3xFL-SRSF7 (22h pretreatment with 1µg/ml doxycycline)-inducible RAW 264.7 macrophages measured by relative light units (RLUs) over time course (Erdman; MOI=1). Data are expressed as a mean of three biological replicates with error bars depicting SEM. Statistical significance was determined using two tailed unpaired student's t test. *=$p<0.05$, **=$p<0.01$, ***=$p<0.001$.

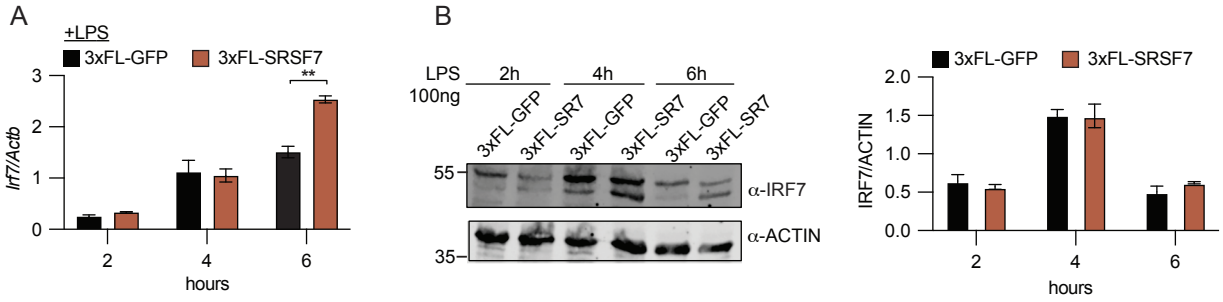
A
+LPS
3xFL-GFP
3xFL-SRSF7
**
Irf7/Actb
3
2
1
0
2
4
6
hours
B
LPS
100ng
2h
4h
6h
3xFL-GFP
3xFL-SR7
3xFL-GFP
3xFL-SR7
3xFL-GFP
3xFL-SR7
55
35
α-IRF7
α-ACTIN
3xFL-GFP
3xFL-SRSF7
IRF7/ACTIN
2.0
1.5
1.0
0.5
0.0
2
4
6
hours

Figure S5: Supplemental data for Figure 5

A. RT-qPCR of *Irf7* in 3xFLAG-GFP (2h dox treatment) or 3xFLAG-SRSF7 (22h dox treatment) inducible RAW 264.7 MΦs over a time course of LPS stimulation (100 ng/ml). **B.** Immunoblot of IRF7 in 3xFLAG-GFP (2h dox treatment) or 3xFLAG-SRSF7 (22h dox treatment) inducible RAW 264.7 cells over a time course of LPS stimulation (100 ng/ml) (quantification right).

375 Having established that decreased levels of IRF7 is the likely culprit for the type I IFN
376 defect in *Srsf7* knockdown MΦs (**Figs. 3-4**) and demonstrated that SRSF7 overexpression is
377 sufficient to promote *Irf7* expression (**Fig. 5**), we set out to determine the mechanism though
378 which SRSF7 controls IRF7 expression. SR proteins play a well-established role in coupling
379 transcription and splicing and have been implicated in transcription by interacting with histone
380 tails (Loomis et al., 2009; Luco et al., 2011; Luco et al., 2010) or by directly mediating transcrip-
381 tional elongation via pTEFb (Ji et al., 2013). To begin to investigate a role for SRSF7 in activat-
382 ing *Irf7* transcription, we performed chromatin immunoprecipitation (ChIP)-qPCR for RNAPII
383 (anti-CTD tail) in *Srsf7* knockdown and SCR control MΦs. We designed primers to tile the *Irf7*
384 promoter region (100bp size amplicon, 100 bp apart from each other (**Fig. 6A**)). We performed
385 ChIP at a 4h time point post-LPS treatment as *Irf7* transcription is induced at this time point and
386 we know the *Srsf7* knockdown phenotype is in play. We observed dramatic accumulation of
387 RNAPII at/around the *Irf7* transcription start site (TSS) (-400 to +250) in *Srsf7* knockdown MΦs
388 (**Fig. 6B**, teal). This pattern of RNAPII in *Srsf7* knockdown MΦs is suggestive of a pile-up result-
389 ing from a failure to convert to a successful elongation complex. We next asked whether this de-
390 fect in RNAPII clearance could be explained by defects in recruitment or retention of transcrip-
391 tion factors like STAT1 to the *Irf7* promoter. Using chromatin immunoprecipitation-qPCR with an
392 antibody against Y701 STAT1, we measured a massive enrichment of STAT1 at the *Irf7* pro-
393 moter in SCR cells at 4h post-LPS (**Fig. 6C**, grey). This STAT1 signal was completely lost in
394 *Srsf7* knockdown MΦs (**Fig. 6C**, teal). An analogous set of ChIP-qPCRs at the promoter of *Ifit3*,
395 another ISG whose expression is SRSF7-dependent, showed no differences in RNAPII or
396 STAT1 occupancy (**Fig. 6D-F**). Likewise, we saw no difference in RNAPII occupancy in *Srsf7*
397 knockdown MΦs versus SCR controls at the *Stat1* promoter (**Fig. 6G-H**). These data support a
398 role for SRSF7 in promoting transcription of *Irf7* and suggest that dampened expression of ISGs
399 like *Ifit3* in *Srsf7* knockdown MΦs occurs indirectly, downstream of IRF7 defects.
400 Having linked STAT1 binding and RNAPII elongation at the *Irf7* promoter to SRSF7, we
401 next asked whether SRSF7 carries out this function by directly associating with the *Irf7* genomic
402 locus. As ChIP-grade antibodies are not available for SRSF7, we turned back to our 3xFLAG-
403 SRSF7 and 3xFLAG-GFP doxycycline-inducible cell lines (**Fig. 5A**) and performed ChIP-qPCR
404 of 3xFLAG-SRSF7 and 3xFLAG-GFP at the *Irf7* promoter using the same primer sets shown in
405 Fig. 6A. We observed significant enrichment of SRSF7 at the *Irf7* promoter (-500 to 0) (3 to 4-fold
406 over 3xFLAG-GFP control) (**Fig. 6I**) and no SRSF7 enrichment at *Ifit3* (**Fig. 6J**). To take an unbi-
407 ased global look at SRSF7 association with the murine genome, we performed ChIP-seq. Data
408 was analyzed by ROSALIND. Briefly, Cutadapt trimmed reads, quality scores were determined

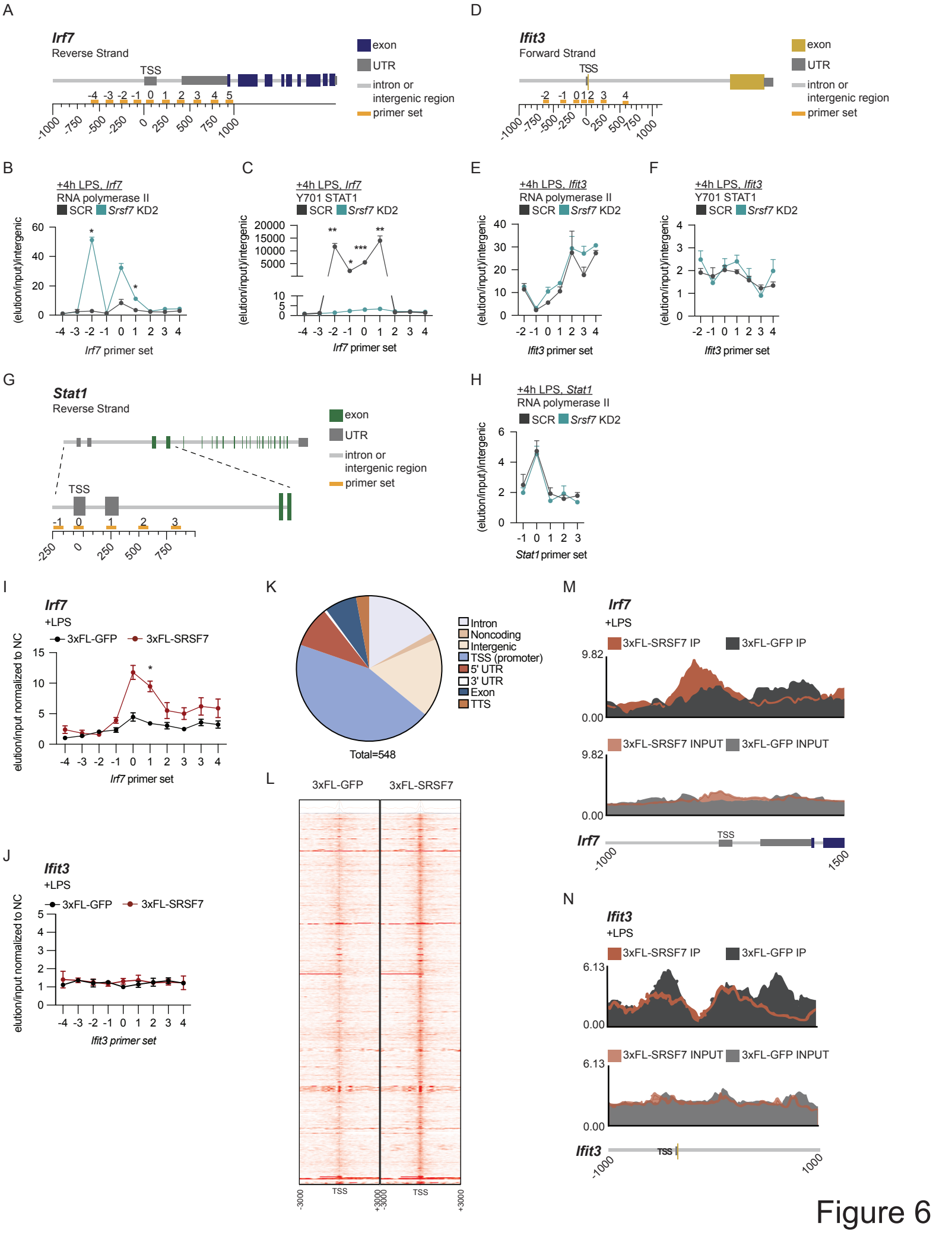
A
Irf7
Reverse Strand
TSS
exon
UTR
intron or intergenic region
primer set
D
Ifit3
Forward Strand
TSS
B
+4h LPS, Irf7
RNA polymerase II
SCR Srsf7 KD2
(elution/input)/intergenic
Irf7 primer set
C
+4h LPS, Irf7
Y701 STAT1
SCR Srsf7 KD2
E
+4h LPS, Ifit3
RNA polymerase II
Ifit3 primer set
F
+4h LPS, Ifit3
Y701 STAT1
G
Stat1
Reverse Strand
H
+4h LPS, Stat1
RNA polymerase II
Stat1 primer set
I
Irf7
+LPS
3xFL-GFP
3xFL-SRSF7
elution/input normalized to NC
Irf7 primer set
K
Intron
Noncoding
Intergenic
TSS (promoter)
5' UTR
3' UTR
Exon
TTS
Total=548
L
3xFL-GFP
3xFL-SRSF7
TSS
M
Irf7
+LPS
3xFL-SRSF7 IP
3xFL-GFP IP
3xFL-SRSF7 INPUT
3xFL-GFP INPUT
J
Ifit3
+LPS
Ifit3 primer set
N
Ifit3
+LPS

Figure 6

Figure 6: SRSF7 promotes STAT1 association and RNA polymerase II elongation by associating with the *Irf7* promoter

A. Schematic diagram of the *Irf7* gene with tiling primers designed around the transcriptional start site (orange). **B.** RNA polymerase II ChIP-qPCR at the *Irf7* promoter in SCR and *Srsf7* KD RAW MΦs 4h post-LPS stimulation (100ng/ml). Data represented as elution/input normalized to that of an intergenic control primer set. **C.** Y701 STAT1 ChIP-qPCR at the *Irf7* promoter in SCR or *Srsf7* KD RAW MΦs 4h post-LPS stimulation (100 ng/ml). Data represented as elution/input normalized to that of an intergenic control. **D.** Schematic diagram of the *Ifit3* gene with tiling primers designed around the transcriptional start site (orange). **E.** As in B but at the *Ifit3* promoter. **F.** As in C but at the *Ifit3* promoter. **G.** Schematic diagram of the *Stat1* gene with tiling primers designed around the transcriptional start site (orange). **H.** As in B but at the *Stat1* promoter. **I.** ChIP-qPCR at the *Irf7* promoter 4h post-LPS (100 ng/ml) in 3xFLAG-GFP and 3xFLAG-SRSF7 dox-inducible RAW 264.7 MΦs. **J.** As in I at the *Ifit3* promoter. **K.** Functional categorization of unique ChIP peaks in 3xFL-SRSF7 dox-inducible RAW 264.7 MΦs 4h post-LPS (100 ng/ml). **L.** Heatmap indicating read coverage density at transcriptional start sites (TSS) in 3xFL-GFP or 3xFL-SRSF7 inducible RAW 264.7 MΦs. **M.** Enrichment of 3xFLAG-SRSF7 and 3xFLAG-GFP at the *Irf7* promoter by ChIP-seq: IP (top) and input (bottom). **N.** As in M but at the *Ifit3* promoter. Data are expressed as a mean of three or more technical replicates with error bars depicting SEM. Statistical significance was determined using two tailed unpaired student's t test. *=$p<0.05$, **=$p<0.01$, ***=$p<0.001$.

A

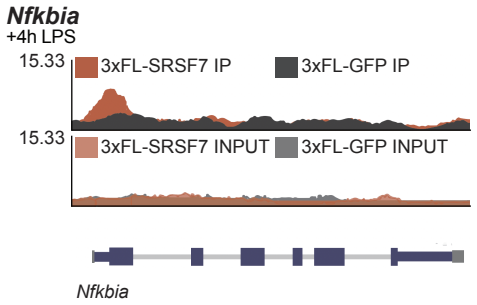

B

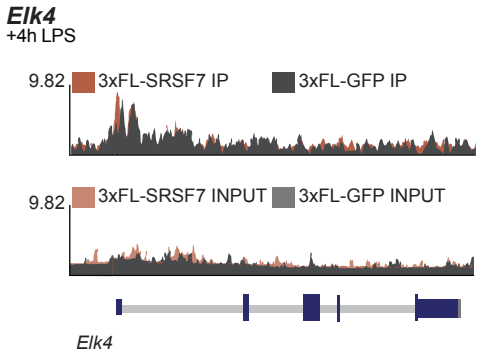

C

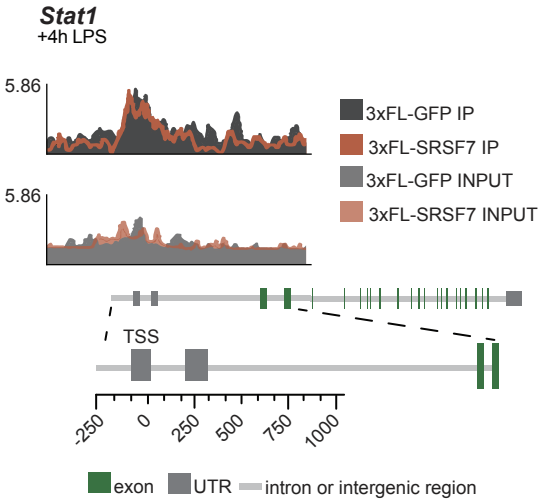

D

Name	P-value	Percent of Targets	Percent of Background
Etv2(ETS)/ES-ER71-ChIP-Seq(GSE59402)/Homer	1e-6	16.79%	9.68%
ZNF41(Zf)/HEK293-ZNF41.GFP-ChIP-Seq(GSE58341)/Homer	1e-6	1.46%	0.11%
Fli1(ETS)/CD8-FLI-ChIP-Seq(GSE20898)/Homer	1e-6	25.36%	17.02%
AT1G76870(Trihelix)/col-AT1G76870-DAP-Seq(GSE60143)/Homer	1e-6	4.93%	1.63%
Elk4(ETS)/Hela-Elk4-ChIP-Seq(GSE31477)/Homer	1e-5	19.34%	12.62%
ETV4(ETS)/HepG2-ETV4-ChIP-Seq(ENCODE)/Homer	1e-4	25.36%	18.08%
ETS(ETS)/Promoter/Homer	1e-4	12.04%	7.09%
ELF1(ETS)/Jurkat-ELF1-ChIP-Seq(SRA014231)/Homer	1e-4	17.34%	11.50%
NAM(NAC)/col-NAM-DAP-Seq(GSE60143)/Homer	1e-4	16.06%	10.71%

Figure S6: Supplemental data for Figure 6

A. Enrichment of 3xFLAG-SRSF7 and 3xFLAG-GFP at the *Nfkbia* promoter by ChIP-seq: IP (top) and input (bottom). **B.** Enrichment of 3xFLAG-SRSF7 and 3xFLAG-GFP at the *Elk4* promoter by ChIP-seq: IP (top) and input (bottom). **C.** Enrichment of 3xFLAG-SRSF7 and 3xFLAG-GFP at the *Irf7* promoter by ChIP-seq: IP (top) and input (bottom). **D.** Putative SRSF7 motifs predicted by HOMER from 3xFLAG-SRSF7 ChIP-seq data.

409 by FASTQC, and reads were aligned to the *Mus musculus* genome build mm10 using Bowtie.
410 After quality control, peaks were called using MACS2 with input/IgG controls background sub-
411 tracted. We detected 548 unique peaks for SRSF7 across the genome, with almost half of these
412 peaks being at transcription start sites (**Fig. 6K-L**), for example at *Nfkbia* (**Fig. S6A**) and *Elk4*
413 (**Fig. S6B**). By ChIP-seq we again saw a clear SRSF7 peak at the *Irf7* promoter compared to GFP
414 (**Fig. 6M**), but not at *Ifit3* (**Fig. 6N**) or *Stat1* (**Fig. S6A**). ChIP-seq data revealed 3xFL-SRSF7
415 enrichment at several immune-associated genes such as *Fos*, *Myd88, Ifitm3*, and *Dusp5*. Inter-
416 estingly, and in support of our model that lack of ISG induction in *Srsf7* knockdown MΦs is driven
417 by defects in *Irf7* expression, we did not see SRSF7 peaks at any other interferon-associated
418 transcription factors. ChIP-seq did not reveal a strong consensus sequence for SRSF7 and con-
419 sensus sequence enrichment was only detected at subsets of genes: Etv2 (ETS) sites (P-value
420 = 1e-6 and 16.79% of targets), ZNF41 (P-value = 1e-6 and 1.46% of targets), Fili1 (ETS) (P-value
421 = 1e-6 and 25.36% of targets), and AT1G76870 (Trihelix) (P-value = 1e-6 and 4.93% of targets)
422 (**Fig. S6D**). These data reveal unexpected roles for the RNA binding protein SRSF7 in associating
423 with gene promoters and in facilitating STAT1 association and RNAPII elongation at the *Irf7* pro-
424 moter.
425
426 **DISCUSSION**
427 Considering the critical role SR/hnRNP family proteins play in regulating many aspects
428 of gene expression, we know surprisingly little about how they shape the transcriptomes of spe-
429 cialized cell types. Here, we describe a novel role for the splicing regulatory protein SRSF7 in
430 stimulating the type I IFN response by activating transcription of the *Irf7* gene. Our data demon-
431 strate that enrichment of SRSF7 at the *Irf7* promoter facilitates association of the transcription
432 factor STAT1 and promotes RNAPII elongation to activate *Irf7* gene expression. By controlling
433 IRF7 abundance, SRSF7 plays a privileged role in regulating both antiviral (**Fig. 2Q-T**) and pro-
434 bacterial (**Fig. 5J**) innate immune responses in macrophages. In addition to implicating SRSF7
435 in activating *Irf7* expression, this work demonstrates a critical and underappreciated role for both
436 SRSF7 and IRF7 in maintaining tonic and early interferon signaling in MΦs.
437 A major finding of this study relates to the ability of SRSF7—a canonical RNA binding
438 protein—to promote transcription of *Irf7*. Over the past two decades, the idea that transcription
439 and RNA processing occur in a linear, stepwise fashion has been repeatedly challenged. It is
440 now generally accepted that many steps in RNA processing (i.e. capping, pre-mRNA splicing,
441 RNA editing) occur co-transcriptionally while nascent transcripts are still bound to RNAPII. Ac-
442 cordingly, splicing can influence transcription and transcription can impact splicing (Tellier et al.,

443 2020). Several studies have linked SR proteins to RNAPII dynamics and co-transcriptional
444 splicing. SRSF2, for example, releases the cyclin-dependent kinase pTEFb from an inhibitory
445 7SK-containing complex to relieve stalled polymerase at promoters (Ji et al., 2013) and SRSF3
446 regulates exon inclusion via the C-terminal domain of RNAPII (de la Mata and Kornblihtt, 2006).
447 Although our data suggest an analogous role for SRSF7 in mediating transcription factor binding
448 and RNAPII elongation at the *Irf7* promoter, several aspects of this mechanism still need to be
449 explored.

450 One outstanding question relates to why we see SRSF7 at certain promoters, like *Irf7*,
451 but not others (**Fig. 6**). We currently do not know whether SRSF7 association with the *Irf7* pro-
452 moter is RNA-dependent. If so, it is possible that specificity is dictated by sequences encoded in
453 exons/introns of genes downstream of SRSF7-sensitive promoters such that nascent RNAs
454 serve as the platform for SRSF7 recruitment. The reported consensus sequence for SRSF7 is
455 GA(C/T)GA(C/T) (Cavaloc et al., 1999) and SRSF7 was shown to bind TGA(T/C)C sequences
456 in its own transcript to regulate poison cassette exon inclusion (Konigs et al., 2020). We can de-
457 tect several potential SRSF7 bindings sites in the first coding exon of *Irf7* (TGACC). Thus, it is
458 possible that SRSF7's association at the *Irf7* promoter occurs by virtue of co-transcriptional
459 binding of exonic splicing enhancers (ESEs) in nascent transcripts. It is also conceivable that
460 SRSF7 associates with the *Irf7* promoter in an RNA-independent, DNA-dependent fashion.
461 SRSF7 is the only SR protein that encodes a Zn-knuckle, and to date, this domain has been
462 shown to enhance the RNA binding activity of SRSF7 (Cavaloc et al., 1999; Cavaloc et al.,
463 1994; Wang et al., 2021)). However, in other proteins, for example TAF1, the largest subunit of
464 the general transcription factor TFIIID, a Zn knuckle encourages DNA binding and promoter oc-
465 cupancy (Curran et al., 2018). It is tempting to speculate that the Zn finger domain in SRSF7
466 could promote its association directly with DNA. Future experiments designed to implicate the
467 Zn knuckle in SRSF7 association with the *Irf7* promoter and/or test the ability of SRSF7 to di-
468 rectly bind DNA will help resolve the molecular mechanisms of SRSF7 promoter enrichment.

469 In addition to linking SRSF7 to *Irf7* expression, our studies revealed an unexpected role
470 for IRF7 in controlling tonic type I IFN expression in resting RAW cells (**Fig. 2A, E**) and MEFs
471 (**Fig. 2M-P**, time 0). These observations challenge the paradigm that IRF7 needs to be upregu-
472 lated before it can contribute to type I IFN responses. Indeed, differences in ISG expression
473 were more robust in IRF7 KO RAW 264.7 MΦs at rest than after LPS stimulation (**Fig. S4B)**.
474 These findings suggest that IRF7 is in fact the major mediator of the type I IFN response in rest-
475 ing macrophages, but *both* IRF3 and IRF7 contribute once they are activated downstream of
476 pattern recognition receptor engagement. To date, the role for IRF7 in maintaining tonic type I

477 IFN signaling has not been fully explored. Our RNA-seq data identify a specific regulon of ISGs
478 that is particularly sensitive to loss of IRF7 at baseline (**Fig. 4D, G**). Among the most downregu-
479 lated genes in resting *Irf7* KO macrophages are several encoding guanylate binding proteins
480 (GBPs) and members of the oligoadenylate synthetase (OAS) family. Regulated expression of
481 these factors at baseline may reflect their role in directly mediating anti-viral and anti-bacterial
482 killing, with low level expression of these ISGs in resting cells providing an early advantage
483 upon infection. By demonstrating a role for IRF7 in maintaining tonic levels of these and other
484 ISGs, our results hint at roles for IRF7 in cellular homeostasis and disease have not been ap-
485 preciated to date.
486 Consistent with this idea, growing evidence suggests that IRF7 expression in immune
487 cells is subject to multiple levels of control mediated by RBPs. Both mouse and human IRF7
488 genes encode very small introns (<100nt), an unusual adaptation in mammalian genomes. Reg-
489 ulated *IRF7* intron retention has been reported in THP-1 cells, wherein intron 2 is efficiently re-
490 moved upon monocyte-to-macrophage differentiation but not in resting monocytes (Green et al.,
491 2020). In response to treatment with TNF-α and IFN-α, as well as polyI:C transfection, regulated
492 removal of IRF7 intron 4 has been reported and was shown to be controlled by the RBP BUD13,
493 which is enriched on *Irf7* transcripts in BMDMs (Frankiw et al., 2019). Such regulation is pro-
494 posed to provide innate cells a way to limit the inappropriate expression of genes with high in-
495 flammatory potential like IRF7, while leaving cells poised to upregulate these genes when cer-
496 tain signals are received. We did not observe differences in the number of intron reads in *Srsf7*
497 KD vs. SCR RAW cells (**Fig. 3H**), nor did the MAJIQ algorithm identify SRSF7-dependent alter-
498 native splicing changes in *Irf7* (**Fig. 1**). We propose that intron retention/alternative splicing of
499 *Irf7* by factors like BUD13 adds an additional layer of regulation on top of the transcriptional con-
500 trol conferred by SRSF7. The fact that IRF7 is subject to regulation at multiple nodes argues
501 that it plays a larger than appreciated role in mediating inflammatory responses in immune cells.
502 Together, these previously published studies and our work presented here, argue that IRF7
503 does more than amplify late interferon responses and highlight a preeminent role for RNA bind-
504 ing proteins in regulating innate immune outcomes.
505
506 **ACKNOWLEDGEMENTS**
507 We would like the thank members of Patrick and Watson labs for critical reading of the manu-
508 script and invaluable feedback. We would also like to thank Phillip West and members of his lab
509 at Texas A&M School of Medicine for sharing reagents and protocols related to VSV infection.
510 Thanks to Susan Carpenter and her lab for sharing reagents and protocols related to iBMDMs.

and to the Genomic and RNA Profiling Core at Baylor, College of Medicine for RNA-seq and ChIP-seq library generation and sequencing.

Materials and Methods

M. tuberculosis

The Erdman strain was used for all *M. tuberculosis* (Mtb) infections as well as Mtb luxBCADE a luciferase expressing strain. Low passage lab stocks were thawed for each experiment to ensure virulence was preserved. Mtb was cultured in roller bottles at 37 °C in Middlebrook 7H9 broth (BD Biosciences) supplemented with 10% OADC (BD Biosciences), 0.5% glycerol (Fisher), and 0.1% Tween-80 (Fisher). All work with Mtb was performed under Biosafety Level 3 containment using procedures approved by the Texas A&M University Institutional Biosafety Committee.

Mtb in vitro infections

To prepare the inoculum, bacteria were grown to mid log phase (OD 0.6–0.8), spun at low speed (500 rcf) to remove clumps, and then pelleted and washed with PBS 2X. Resuspended bacteria were sonicated and spun at low speed again to further remove clumps. Then Mtb was then diluted in DMEM plus 10% horse serum (Gibco) and added to cells at a multiplicity of infection (MOI) of 10 for RNA and protein analysis, a MOI of 5 for cell death studies, and a MOI of 1 for bacterial growth assays. The day before the infection, RAW 264.7 macrophages were plated on 12-well tissue culture–treated plates at a density of 3×10^5 cells per well or plated in corning 96 well black plates at $2.5\text{x}10^4$ cells/well and allowed to rest overnight. Cells were spun with bacteria for 10 min at 1,000 rcf to synchronize infection, washed 2X with PBS, and then incubated in fresh media. Where applicable, RNA was harvested from infected cells using 0.25 ml TRIzol reagent at each time point. For bacterial growth assays RAW 264.7 macrophages were plated on 12-well tissue culture–treated plates at a density of 2.5×10^5 cells per well. Luminescence was read for *M. tuberculosis luxBCADE* by lysing in 250 µl 0.5% Triton X-100 and dividing sample into duplicate wells of a 96-well white bottomed plate (Costar). Luminescence was measured and normalized to background using the luminescence feature of the INFINITE 200 PRO (Tecan) at 0, 48, 72 and 92 h post infection.

S. enterica (ser. Typhimirium)

Salmonella enterica serovar Typhimurium (SL1344) was obtained from Dr. Denise Monack, Stanford. S. T. stocks were streaked out on LB agar plates and incubated at 37°C overnight.

S. enterica (ser. Typhimirium) infections:

RAW 264.7 macrophages were seeded in 12-well tissue culture-treated plates at a density of $7\text{x}10^5$ cells per cell, and cultures of *S. Typhimurium* were grown at 37°C in LB broth containing 0.3M NaCl 16h prior to infection. Bacterial cultures were diluted 1:20 3h prior to infection to reach mid-log phase OD_{600} 0.6-0.8. Mid-log phase bacteria were washed 3x with PBS and pelleted at 5,000 rpm for 3 min. Bacteria were then added to DMEM (Hyclone) with 10% FBS (Sigma) and 2% HEPES (HyClone) at an MOI of 5 for transcripts and MOI of 1 for replication. Infected cells were spun at 1,000 rpm for 5 min then incubated for 10 min at 37 °C prior to gentamycin washes adding fresh media. At indicated times post infection, cells were harvested with TRIzol for RNA isolation described below.

Vesicular stomatitis virus

Recombinant *Vesicular stomatitis* virus (VSV; Indiana serotype) containing a GFP reporter cloned downstream of the VSV G-glycoprotein (VSV-G/GFP) was obtained collaboratively from Dr. John Rose at Yale School of Medicine though Dr. A. Phillip West at Texas A&M Health Science Center.

Vesicular stomatitis Virus (VSV) infections

1100 RAW 264.7 macrophages were seeded in 12-well tissue culture-treated plates at a density of
1101 $7x10^5$ cells per well 16h before infection. The next day cells were infected with VSV-GFP virus
1102 (Dalton and Rose, 2001) at an MOI of 0.1 in serum-free DMEM (HyClone). After 1h of incuba-
1103 tion with media containing virus, supernatant was removed, and fresh DMEM plus 10% FBS
1104 (Millipore) was added to each well. At indicated times post infection, cells were harvested with
1105 TRIzol for RNA isolation described below.
1106
1107 *M. musculus*
1108 Mice used in this study were C57BL6/J (Stock #00064) initially purchased from Jackson Labra-
1109 tory and afterward maintained with filial breeding. All mice used in experiments were compared
1110 to age- and sex- matched controls. Littermates were used for experiments. Mice used to gener-
1111 ate BMDMs were males between 10-16 weeks old. Embryos used to make primary MEFs were
1112 14.5 days post-coitum. All animals were housed, bred, and studied at Texas A&M Health Sci-
1113 ence Center under approved Institutional Care and Use Committee guidelines. All experiments
1114 for this study were reviewed and approved by the Texas A&M University Institutional Animal
1115 Care and Use Committee (AUP# 2019–0083). Mice were fed 4% standard chow and were kept
1116 on a 12 h light/dark cycle and provided food and water *ad libitum*. Mice were group housed
1117 (maximum 5 per cage) by sex on ventilated racks in temperature-controlled rooms.
1118
1119 Primary cell culture
1120 Bone marrow derived macrophages (BMDMs) were differentiated from bone marrow (BM) cells
1121 isolated by washing mouse femurs with 10 ml DMEM 1 mM sodium pyruvate. Cells were then
1122 centrifuged for 5 min at 400 rcf and resuspended in BMDM media (DMEM, 20% FBS (Millipore),
1123 1 mM sodium pyruvate (Lonza), 10% MCSF conditioned media (Watson lab)). BM cells were
1124 counted and plated at $5x10^6$ cells per 15 cm non-tissue culture treated dishes in 30 ml complete
1125 BMDM media. Cells were fed with an additional 15 ml of BMDM media on day 3. Cells were har-
1126 vested on day 7 with 1X PBS EDTA (Lonza).
1127 Mouse embryonic fibroblasts (MEFs) were isolated from embryos. Briefly, embryos were dis-
1128 sected from yolk sacs, washed two times with cold 1X PBS, decapitated, and stripped of perito-
1129 neal contents. Headless embryos were disaggregated in cold 0.05% trypsin-EDTA (Lonza) and
1130 incubated on ice for 20 min., followed by incubation at 37 °C for an additional 20 min. Cells were
1131 then DNase treated with 4 ml disaggregation media (DMEM, 10% FBS, 100 µg/ml DNASE I
1132 (Worthington)) for 20 min at 37 °C. Isolated supernatants were spun down at 1000 rpm for 5
1133 min. Cells were resuspended in complete MEF media (DMEM, 10% FBS, 1 mM sodium py-
1134 ruvate), and plated in 15 cm tissue culture-treated dishes 1 dish per embryo in 25 ml of media.
1135 MEFs were allowed to expand for 2-3 days before harvest with 0.05% trypsin-EDTA (Lonza).
1136 iBMDMs were immortalized with J2 virus to generate iBMDMs.
1137
1138 Cell culture
1139 RAW 264.7 macrophages (TIB-71™ ATCC) (originally isolated from male BALB/c mice), L929
1140 ISRE (Hoffpauir et al., 2020), *Irf7* KO RAW 264.7 macrophages (this paper), and Lenti-X cells
1141 (TaKaRa Bio) were cultured at 37 °C with a humidified atmosphere of 5% CO_2 in complete me-
1142 dia containing high glucose, DMEM (ThermoFisher) with 10% FBS (Millipore) 0.2% HEPES
1143 (Thermo Fisher).
1144
1145 shRNA knockdowns
1146 For RAW 264.7 macrophages stably expressing scramble knockdown and *Srsf7* knockdown,
1147 Lenti-X cells were transfected with a pSICO scramble non-targeting shRNA construct and
1148 pSICO *Srsf7* shRNA constructs targeted at exon 3 and exon 4 of *Srsf7* using Polyjet (SignaGen
1149 Laboratories). Virus was collected 24 and 48 h post transfection. RAW 264.6 macrophages

1150 were transduced using Lipofectamine 2000 (Thermo Fischer). After 48 h, media was supple-
1151 mented with Hygromycin (Invitrogen) to select for cells containing the shRNA plasmid.
1152
1153 siRNA knockdowns in MEFs
1154 Knockdown of mRNA transcripts was performed by plating $3x10^6$ MEFs in 10 cm plates and
1155 rested overnight. The following day complete media was replaced with 5 ml fresh complete me-
1156 dia 30 min prior to transfection. Cells were transfected using Fugene SI reagent 10 µM of siRNA
1157 stock against either *Srsf7* (ThermoFisher, s105011) or negative control, Silencer® Select Nega-
1158 tive Control #1 (4390843). Cells were incubated for 48h in transfection media at 37 °C with 5%
1159 CO_2 prior to downstream experiments.
1160
1161 siRNA knockdowns in BMDMs
1162 The day prior to transfection, 6x10e5 BMDMs were seeded into 12-well plates. The day of trans-
1163 fection, 50nM of siRNA against *Srsf7* (ThermoFisher, s105011) or negative control, Silencer®
1164 Select Negative Control #1 (4390843) were mixed with 3 µl of LipoRNAiMAX (13778150,
1165 Thermo Fisher Scientific), incubated for 10m at room temperature, and then added into wells
1166 with 500 µl plain DMEM. Transfection proceeded for 6h and then wells were replenished with
1167 complete media.
1168
1169 Tetracycline inducible cell line generation
1170 For generation of tetracycline inducible RAW 264.7 macrophages, pLenti CMV rtTA3 Blast
1171 (Addgene w756-1) stably expressing clonal RAW 264.7 macrophages were transduced with
1172 pLenti CMV Puro DEST (Addgene w118-1) constructs containing 3xFL-GFP, 3xFL-SRSF7, and
1173 al 3xFL-SRSF7 phosphorylation mutants. After 48 h construct containing cells were selected
1174 through addition of puromycin (Invivogen). 1 mg/ml doxycycline (Sigma-Aldrich) treatment was
1175 used to activate construct expression.
1176
1177 Cell stimulation for immune activation
1178 $7.5x10^5$ RAW 264.7 macrophage were plated on 12-well tissue-culture treated plates 16h before
1179 cellular stimulation assays. The next day, cells were treated with lipopolysaccharide (LPS) from
1180 *E. coli* (Invivogen) at 100 ng/ml, or ISD (IDT, annealed in house) at 1 µg/ml, or IFNβ (PBL Assay
1181 Science) at 200 I/U per ml for the respective time points. Cells were collected for RNA isolation
1182 using Trizol reagent.
1183
1184 *Srsf7* KD mRNA sequencing and analysis
1185 As reported in Wagner, Scott and West et al. 2021, RNA-seq analysis was performed on RAW
1186 264.7 cells containing shRNA knockdowns of *Srsf6*, *Srsf2*, *Srsf1*, *Srsf7*, and *Srsf9* compared to
1187 SCR control with biological triplicates of each cell line. RNA-Seq and library preparation was
1188 performed by Texas A&M AgriLife Genomics and Bioinformatics Service. RNA samples were
1189 sequenced on Illumina 4000 using 2 × 150-bp paired-end reads. Raw reads were filtered and
1190 trimmed and Fastq data was mapped to the Mus musculus Reference genome (RefSeq) using
1191 CLC Genomics Workbench 8.0.1. Differential expression analyses were performed using CLC
1192 Genomics Workbench. Relative transcript expression was calculated by counting Reads Per
1193 Kilobase of exon model per Million mapped reads (RPKM). Statistical significance was deter-
1194 mined by the EDGE test *via* CLC Genomics Workbench. Differentially expressed genes (DEGs)
1195 were selected as those with p value threshold < 0.05. Critical pathways affected by SR protein
1196 knockdown compared to control RAW 264.7 macrophages, were analyzed by canonical path-
1197 way analysis using Ingenuity Pathway Analysis software from QIAGEN Bioinformatics. Genes
1198 that were differentially expressed with a p-value < 0.05 from our RNA-SEQ analysis were used
1199 as input. Integrated genomics viewer (IGV) visualization tracks were generated using the RNA-
1200 SEQ filtered and trimmed reads.

1201
1202 *Irf7* KO mRNA sequencing and analysis
1203 RNA- seq analysis was performed on control GFP KO or *Irf7* KO1 RAW 264.7 cells in biological
1204 triplicate of each cell line. Data was analyzed by ROSALIND® (https://rosalind.bio/), with a
1205 HyperScale architecture developed by ROSALIND, Inc. (San Diego, CA). Reads were trimmed
1206 using cutadapt[1]. Quality scores were assessed using FastQC[2]. Reads were aligned to the Mus
1207 musculus genome build GRCm39 using STAR[3]. Individual sample reads were quantified using
1208 HTseq[4] and normalized via Relative Log Expression (RLE) using DESeq2 R library[5]. Read Dis-
1209 tribution percentages, violin plots, identity heatmaps, and sample MDS plots were generated as
1210 part of the QC step using RSeQC[6]. DEseq2 was also used to calculate fold changes and p-val-
1211 ues and perform optional covariate correction. Clustering of genes for the final heatmap of dif-
1212 ferentially expressed genes was done using the PAM (Partitioning Around Medoids) method us-
1213 ing the fpc R library[7]. Hypergeometric distribution was used to analyze the enrichment of path-
1214 ways, gene ontology, domain structure, and other ontologies. The topGO R library[8,] was used to
1215 determine local similarities and dependencies between GO terms in order to perform Elim prun-
1216 ing correction.
1217
1218 Alternative splicing analysis
1219 Modeling Alternative Junction Inclusion Quantification (MAJIQ) and the Voila visualization pack-
1220 age were used to model alternative splicing events with default parameters described by
1221 Vaquero-Garcia et al., 2016. Junction-spanning reads were used to construct splice graphs for
1222 transcripts by using the RefSeq annotation supplemented with de-novo (junctions not in the Ref-
1223 Seq transcriptome database but had sufficient evidence in the RNAseq data) detected junctions.
1224 Resulting splice graphs were analyzed for all identified local splice variations (LSVs). MAJIQ
1225 then quantified expected percent spliced in (PSI) value in control and knockdown samples for
1226 every junction in each LSV. Resulted viewed on VOILA were filtered for highest confidence
1227 change in LSVs (one or more junctions had at least a 95% probability of expected dPSI of at
1228 least an absolute value of 0.2 PSI units between control and knockdown.
1229
1230 RNA isolation and qPCR analysis
1231 For transcript analysis, cells and tissue were harvested in TRIzol and RNA was isolated using
1232 Direct-zol RNA Miniprep kits (Zymo Research) with 1 h DNase treatment. cDNA was synthe-
1233 sized with iScript cDNA Synthesis Kit (Bio-Rad). CDNA was diluted as appropriate for treatment,
1234 and a pool of cDNA was used to make a 1:3 standard curve with each standard sample diluted
1235 1:5 to produce a linear curve. RT-qPCR was performed using Power-Up SYBR Green Master
1236 Mix (Thermo Fisher) using a Quant Studio Flex6 (Applied Biosystems). Samples were run in
1237 triplicate wells in a 384-well plate. Averages of the raw values were normalized to average val-
1238 ues for the same sample with the control gene, *Actb*.
1239
1240 Semiquantitative qPCR analysis
1241 cDNA was synthesized by iScript cDNA Synthesis Kit (Bio-Rad) using an extended 1h amplifica-
1242 tion. Q5 high fidelity 2X Master mix (New England Biolabs) was used for PCR amplification us-
1243 ing targeted primers. Loading dye was added to PCR products and samples were run on 2%
1244 agarose gel containing ethidium bromide at 100 volts for 1 h. Gels were imaged on LiCOR Od-
1245 yssey Fc Dual-Mode Imaging System and bands were quantified.
1246
1247 Chromatin immunoprepitation
1248 $6x10^6$ RAW 264.7 cells or BMDMs were seeded in a 10 cm dish, and 16h later stimulated for the
1249 indicated time. After stimulation cells were scraped, transferred to a 50 ml conical and fixed with
1250 1% (v/v) formaldehyde for 10 min with gentle shaking. Formaldehyde was quenched with 0.125
1251 M glycine for 5 min. Cells were pelleted and washed 1x with PBS, and then cells were lysed in 1

1252 ml of ChIP lysis buffer (150 mM NaCl, 5 mM EDTA, 0.5% NP-40 and 1% Triton X-100, 50 mM
1253 Tris-HCl, and protease/phosphatase inhibitor (added immediately before lysis) pH 7.5). Lysates
1254 were flash frozen, or ChIP proceeded by sonicating with for 40 min (30 sec on/off 10 min cycles)
1255 in a Bioruptor UCD-200 (Diagenode). Lysates were cleared and 10% taken for input samples.
1256 Endogneous ChIP**:** For RNA polymerase 2 samples: 2 µg of the anti-pol II (Active Motif) or 2 µg
1257 of isotype control (IgG, Cell Signaling) were incubated overnight at 4 with rotation. The following
1258 day, Piece beads (Invitrogen) were washed 3x in ChIP buffer, blocked for 30 min with 100 µg
1259 salmon sperm DNA (Invitrogen) and 0.5 mg BSA, and washed once more with ChIP lysis buffer.
1260 Blocked beads were incubated with cleared chromatin immunocomplexes for 1h at 4 °C with ro-
1261 tation. Beads were washed five times with ChIP buffer and then eluted with 250 µl of elution
1262 buffer (1% SDS and 0.1 M $NaHCO_3$) at 65 °C for 15 mins. The eluate and input were centrifuged
1263 and reverse the cross-links by adding 0.4 M NaCl for overnight at 55 °C. The next day, 1 µl of
1264 RNASE A (10 mg/ml, ThermoFisher) and 2 µl proteinase K (20 mg/ml, ThermoFisher) were
1265 added to the samples and incubated for 1h at 55 °C while shaking. Samples were then sub-
1266 jected to Genomic Clean up and Concentrator (Zymo) to extract DNA. Purified input and IP DNA
1267 were analyzed by qRT-PCR using primers specific for the promoter region of target genes. Re-
1268 sults were normalized to input. Data is presented as fold enrichment relative to intergenic con-
1269 trol. Flag ChIP**:** As above except cleared lysates were added to blocked (as above) M2 anti-
1270 3xFLAG beads and protocol proceeded as above.
1271
1272 3x-FLAG ChIPseq
1273 Data was analyzed by ROSALIND® (https://rosalind.bio/), with a HyperScale architecture devel-
1274 oped by ROSALIND, Inc. (San Diego, CA). Reads were trimmed using cutadapt[1]. Quality scores
1275 were assessed using FastQC[2]. Reads were aligned to the Mus musculus genome build mm10
1276 using bowtie2[3]. Per-sample quality assessment plots were generated with HOMER[4] and Mosa-
1277 ics[5]. Peaks were called using MACS2[6] (with input/IgG controls background subtracted, if pro-
1278 vided). Peak overlaps and differential binding were calculated using the DiffBind R library[7]. Dif-
1279 ferential binding was calculated at gene promoter sites. Read distribution percentages, identity
1280 heatmaps, and FRiP plots were generated as part of the QC step using ChIPQC R library[8] and
1281 HOMER. HOMER was also used to generate known and de novo motifs and perform functional
1282 enrichment analysis of pathways, gene ontology, domain structure and other ontologies.
1283
1284 CRISPR/Cas9 KO of *Irf7*
1285 Guide RNAs were generated to target the 3rd exon of *Irf7* using the Broad online tool
1286 (https://portals.broadinstitute.org/gppx/crispick/public) and synthesized by IDT. Primers were
1287 cloned into digested vector by phosphorylating, annealing, and ligating primers into LentiGuide-
1288 Puro (Addgene, plasmid 52963). Colonies were validated by Sanger sequencing using
1289 pLK0.1/hU6 promoter primer (Eton Biosciences, San Diego, CA). Lentivirus with sgRNAs were
1290 produced and used to transduce RAW 264.7 cells stably expressing FL-Cas9 (Addgene, plas-
1291 mid 52962). After selection with 5 µg/ml puromycin knockout efficiency was analyzed by im-
1292 munoblot and then sequencing for mutants by amplifying a 300 base pair region of genomic
1293 DNA around exon 3. These PCR fragments were sequenced (as above) and compared to con-
1294 trols using TIDE analysis. The two best, most efficient sgRNA populations were clonally se-
1295 lected, expanded, and assayed for clones with total KO of IRF7 by immunoblot.
1296
1297 Protein quantification by immunoblot
1298 Cells were washed with PBS and lysed in 1X RIPA buffer with protease and phosphatase EDTA
1299 free inhibitors (Thermo Scientific), with the addition of 1 U/ml Benzonase (Millipore) to degrade
1300 genomic DNA. Proteins were separated by SDS-PAGE on AnykD mini -PROTEAN TGX precast
1301 gel (Bio-Rad) and transferred to 0.45µm nitrocellulose membranes (GE Healthcare). Mem-
1302 branes were blocked for 1h at RT in TBS +5% BSA. Blots were incubated overnight at 4 °C with

1303 the following primary antibodies: β-ACTIN (Abcam, 1:5000), Y701 STAT1 (Cell Signaling,
1304 1:1000), STAT1 (Cell Signaling, 1:1000), IRF7 (Cell Signaling, 1:1000), SRSF7 (Bethyl 1:3000)
1305 ZBP1 (Santa Cruz Biotechnologies, 1:1000), p-IRF3(S396) (Cell Signaling, 1:1000); IRF3
1306 (Bethyl, 1:1000); ANTI-FLAG M2 (Sigma Aldrich, 1:5000); Membranes were washed 3X for 5
1307 min in PBS-Tween20 and incubated with appropriate secondary antibodies (LI-COR) for 1h at
1308 RT prior to imaging on a LiCOR Odyssey Fc Dual-Mode Imaging System.
1309
1310 Quantitation and Statistical Analysis
1311 Statistical analysis of data was performed using GraphPad Prism software. Two-tailed unpaired
1312 Student's t tests were used for statistical analyses, and unless otherwise noted, all results are
1313 representative of at least three biological samples (mean +/- SEM (n = 3 per group)).
1314
1315
1316

REFERENCES

Barrat, F.J., Crow, M.K., and Ivashkiv, L.B. (2019). Interferon target-gene expression and epigenomic signatures in health and disease. Nat Immunol *20*, 1574-1583.

Bell, S.L., Lopez, K.L., Cox, J.S., Patrick, K.L., and Watson, R.O. (2021). Galectin-8 Senses Phagosomal Damage and Recruits Selective Autophagy Adapter TAX1BP1 To Control Mycobacterium tuberculosis Infection in Macrophages. mBio *12*, e0187120.

Budzik, J.M., Swaney, D.L., Jimenez-Morales, D., Johnson, J.R., Garelis, N.E., Repasy, T., Roberts, A.W., Popov, L.M., Parry, T.J., Pratt, D.*, et al.* (2020). Dynamic post-translational modification profiling of Mycobacterium tuberculosis-infected primary macrophages. Elife *9*.

Cavaloc, Y., Bourgeois, C.F., Kister, L., and Stevenin, J. (1999). The splicing factors 9G8 and SRp20 transactivate splicing through different and specific enhancers. RNA *5*, 468-483.

Cavaloc, Y., Popielarz, M., Fuchs, J.P., Gattoni, R., and Stevenin, J. (1994). Characterization and cloning of the human splicing factor 9G8: a novel 35 kDa factor of the serine/arginine protein family. EMBO J *13*, 2639-2649.

Colwill, K., Pawson, T., Andrews, B., Prasad, J., Manley, J.L., Bell, J.C., and Duncan, P.I. (1996). The Clk/Sty protein kinase phosphorylates SR splicing factors and regulates their intranuclear distribution. EMBO J *15*, 265-275.

Curran, E.C., Wang, H., Hinds, T.R., Zheng, N., and Wang, E.H. (2018). Zinc knuckle of TAF1 is a DNA binding module critical for TFIID promoter occupancy. Sci Rep *8*, 4630.

de la Mata, M., and Kornblihtt, A.R. (2006). RNA polymerase II C-terminal domain mediates regulation of alternative splicing by SRp20. Nat Struct Mol Biol *13*, 973-980.

Duncan, P.I., Howell, B.W., Marius, R.M., Drmanic, S., Douville, E.M., and Bell, J.C. (1995). Alternative splicing of STY, a nuclear dual specificity kinase. J Biol Chem *270*, 21524-21531.

Fitzgerald, K.A., Rowe, D.C., Barnes, B.J., Caffrey, D.R., Visintin, A., Latz, E., Monks, B., Pitha, P.M., and Golenbock, D.T. (2003). LPS-TLR4 signaling to IRF-3/7 and NF-kappaB involves the toll adapters TRAM and TRIF. J Exp Med *198*, 1043-1055.

Frankiw, L., Majumdar, D., Burns, C., Vlach, L., Moradian, A., Sweredoski, M.J., and Baltimore, D. (2019). BUD13 Promotes a Type I Interferon Response by Countering Intron Retention in Irf7. Mol Cell *73*, 803-814 e806.

Gao, D., Ciancanelli, M.J., Zhang, P., Harschnitz, O., Bondet, V., Hasek, M., Chen, J., Mu, X., Itan, Y., Cobat, A.*, et al.* (2021). TLR3 controls constitutive IFN-beta antiviral immunity in human fibroblasts and cortical neurons. J Clin Invest *131*.

Gough, D.J., Messina, N.L., Clarke, C.J., Johnstone, R.W., and Levy, D.E. (2012). Constitutive type I interferon modulates homeostatic balance through tonic signaling. Immunity *36*, 166-174.

Green, I.D., Pinello, N., Song, R., Lee, Q., Halstead, J.M., Kwok, C.T., Wong, A.C.H., Nair, S.S., Clark, S.J., Roediger, B.*, et al.* (2020). Macrophage development and activation involve coordinated intron retention in key inflammatory regulators. Nucleic Acids Res *48*, 6513-6529.

1367 Gu, J., Shi, J., Wu, S., Jin, N., Qian, W., Zhou, J., Iqbal, I.G., Iqbal, K., Gong, C.X., and Liu, F.
1368 (2012). Cyclic AMP-dependent protein kinase regulates 9G8-mediated alternative splicing of tau
1369 exon 10. FEBS Lett *586*, 2239-2244.
1370
1371 Gu, L., Casserly, D., Brady, G., Carpenter, S., Bracken, A.P., Fitzgerald, K.A., Unterholzner, L.,
1372 and Bowie, A.G. (2022). Myeloid cell nuclear differentiation antigen controls the pathogen-
1373 stimulated type I interferon cascade in human monocytes by transcriptional regulation of IRF7.
1374 Nat Commun *13*, 14.
1375
1376 Gui, J.F., Lane, W.S., and Fu, X.D. (1994). A serine kinase regulates intracellular localization of
1377 splicing factors in the cell cycle. Nature *369*, 678-682.
1378
1379 Hoffpauir, C.T., Bell, S.L., West, K.O., Jing, T., Wagner, A.R., Torres-Odio, S., Cox, J.S., West,
1380 A.P., Li, P., Patrick, K.L.*, et al.* (2020). TRIM14 Is a Key Regulator of the Type I IFN Response
1381 during Mycobacterium tuberculosis Infection. J Immunol *205*, 153-167.
1382
1383 Honda, K., and Taniguchi, T. (2006). IRFs: master regulators of signalling by Toll-like receptors
1384 and cytosolic pattern-recognition receptors. Nat Rev Immunol *6*, 644-658.
1385
1386 Honda, K., Yanai, H., Negishi, H., Asagiri, M., Sato, M., Mizutani, T., Shimada, N., Ohba, Y.,
1387 Takaoka, A., Yoshida, N.*, et al.* (2005). IRF-7 is the master regulator of type-I interferon-
1388 dependent immune responses. Nature *434*, 772-777.
1389
1390 Huang, R., Grishagin, I., Wang, Y., Zhao, T., Greene, J., Obenauer, J.C., Ngan, D., Nguyen,
1391 D.T., Guha, R., Jadhav, A.*, et al.* (2019). The NCATS BioPlanet - An Integrated Platform for
1392 Exploring the Universe of Cellular Signaling Pathways for Toxicology, Systems Biology, and
1393 Chemical Genomics. Front Pharmacol *10*, 445.
1394
1395 Jefferies, C.A. (2019). Regulating IRFs in IFN Driven Disease. Front Immunol *10*, 325.
1396 Jeong, S. (2017). SR Proteins: Binders, Regulators, and Connectors of RNA. Mol Cells *40*, 1-9.
1397
1398 Ji, X., Zhou, Y., Pandit, S., Huang, J., Li, H., Lin, C.Y., Xiao, R., Burge, C.B., and Fu, X.D.
1399 (2013). SR proteins collaborate with 7SK and promoter-associated nascent RNA to release
1400 paused polymerase. Cell *153*, 855-868.
1401
1402 Kadota, Y., Jam, F.A., Yukiue, H., Terakado, I., Morimune, T., Tano, A., Tanaka, Y., Akahane,
1403 S., Fukumura, M., Tooyama, I.*, et al.* (2020). Srsf7 Establishes the Juvenile Transcriptome
1404 through Age-Dependent Alternative Splicing in Mice. iScience *23*, 100929.
1405
1406 Kajigaya, H., Ishibashi, T., Hayashi, A., Yamaguchi, Y., and Baba, H. (2016). Concentration of
1407 neddylation-related molecules in paranodal myelin of the peripheral nervous system. Proc Jpn
1408 Acad Ser B Phys Biol Sci *92*, 56-68.
1409
1410 Konigs, V., de Oliveira Freitas Machado, C., Arnold, B., Blumel, N., Solovyeva, A., Lobbert, S.,
1411 Schafranek, M., Ruiz De Los Mozos, I., Wittig, I., McNicoll, F.*, et al.* (2020). SRSF7 maintains its
1412 homeostasis through the expression of Split-ORFs and nuclear body assembly. Nat Struct Mol
1413 Biol *27*, 260-273.
1414
1415 Loomis, R.J., Naoe, Y., Parker, J.B., Savic, V., Bozovsky, M.R., Macfarlan, T., Manley, J.L., and
1416 Chakravarti, D. (2009). Chromatin binding of SRp20 and ASF/SF2 and dissociation from mitotic
1417 chromosomes is modulated by histone H3 serine 10 phosphorylation. Mol Cell *33*, 450-461.

1418 Luco, R.F., Allo, M., Schor, I.E., Kornblihtt, A.R., and Misteli, T. (2011). Epigenetics in
1419 alternative pre-mRNA splicing. Cell *144*, 16-26.
1420
1421 Luco, R.F., Pan, Q., Tominaga, K., Blencowe, B.J., Pereira-Smith, O.M., and Misteli, T. (2010).
1422 Regulation of alternative splicing by histone modifications. Science *327*, 996-1000.
1423
1424 Muller-McNicoll, M., Botti, V., de Jesus Domingues, A.M., Brandl, H., Schwich, O.D., Steiner,
1425 M.C., Curk, T., Poser, I., Zarnack, K., and Neugebauer, K.M. (2016). SR proteins are NXF1
1426 adaptors that link alternative RNA processing to mRNA export. Genes Dev *30*, 553-566.
1427
1428 Nau, G.J., Richmond, J.F., Schlesinger, A., Jennings, E.G., Lander, E.S., and Young, R.A.
1429 (2002). Human macrophage activation programs induced by bacterial pathogens. Proc Natl
1430 Acad Sci U S A *99*, 1503-1508.
1431
1432 Ning, S., Pagano, J.S., and Barber, G.N. (2011). IRF7: activation, regulation, modification and
1433 function. Genes Immun *12*, 399-414.
1434
1435 Pandey, A., Ding, S.L., Qin, Q.M., Gupta, R., Gomez, G., Lin, F., Feng, X., Fachini da Costa, L.,
1436 Chaki, S.P., Katepalli, M.*, et al.* (2017). Global Reprogramming of Host Kinase Signaling in
1437 Response to Fungal Infection. Cell Host Microbe *21*, 637-649 e636.
1438
1439 Patrick, K.L., Bell, S.L., and Watson, R.O. (2016). For Better or Worse: Cytosolic DNA Sensing
1440 during Intracellular Bacterial Infection Induces Potent Innate Immune Responses. J Mol Biol
1441 *428*, 3372-3386.
1442
1443 Schoggins, J.W. (2019). Interferon-Stimulated Genes: What Do They All Do? Annu Rev Virol *6*,
1444 567-584.
1445
1446 Schoggins, J.W., and Rice, C.M. (2011). Interferon-stimulated genes and their antiviral effector
1447 functions. Curr Opin Virol *1*, 519-525.
1448
1449 Schoggins, J.W., Wilson, S.J., Panis, M., Murphy, M.Y., Jones, C.T., Bieniasz, P., and Rice,
1450 C.M. (2011). A diverse range of gene products are effectors of the type I interferon antiviral
1451 response. Nature *472*, 481-485.
1452
1453 Sin, W.X., Yeong, J.P., Lim, T.J.F., Su, I.H., Connolly, J.E., and Chin, K.C. (2020). IRF-7
1454 Mediates Type I IFN Responses in Endotoxin-Challenged Mice. Front Immunol *11*, 640.
1455 Tellier, M., Maudlin, I., and Murphy, S. (2020). Transcription and splicing: A two-way street.
1456 Wiley Interdiscip Rev RNA *11*, e1593.
1457
1458 Vaquero-Garcia, J., Barrera, A., Gazzara, M.R., Gonzalez-Vallinas, J., Lahens, N.F.,
1459 Hogenesch, J.B., Lynch, K.W., and Barash, Y. (2016). A new view of transcriptome complexity
1460 and regulation through the lens of local splicing variations. Elife *5*, e11752.
1461
1462 Wagner, A.R., Scott, H.M., West, K.O., Vail, K.J., Fitzsimons, T.C., Coleman, A.K., Carter, K.E.,
1463 Watson, R.O., and Patrick, K.L. (2021). Global Transcriptomics Uncovers Distinct Contributions
1464 From Splicing Regulatory Proteins to the Macrophage Innate Immune Response. Front Immunol
1465 *12*, 656885.
1466

1467 Wagner, A.R., Weindel, C.G., West, K.O., Scott, H.M., Watson, R.O., and Patrick, K.L. (2022).
1468 SRSF6 balances mitochondrial-driven innate immune outcomes through alternative splicing of
1469 BAX. Elife *11*.
1470
1471 Wagner, R.E., and Frye, M. (2021). Noncanonical functions of the serine-arginine-rich splicing
1472 factor (SR) family of proteins in development and disease. Bioessays *43*, e2000242.
1473
1474 Wang, Y., Yu, Y., Pang, Y., Yu, H., Zhang, W., Zhao, X., and Yu, J. (2021). The distinct roles of
1475 zinc finger CCHC-type (ZCCHC) superfamily proteins in the regulation of RNA metabolism.
1476 RNA Biol *18*, 2107-2126.
1477
1478 Watson, R.O., Bell, S.L., MacDuff, D.A., Kimmey, J.M., Diner, E.J., Olivas, J., Vance, R.E.,
1479 Stallings, C.L., Virgin, H.W., and Cox, J.S. (2015). The Cytosolic Sensor cGAS Detects
1480 Mycobacterium tuberculosis DNA to Induce Type I Interferons and Activate Autophagy. Cell
1481 Host Microbe *17*, 811-819.
1482
1483 West, K.O., Scott, H.M., Torres-Odio, S., West, A.P., Patrick, K.L., and Watson, R.O. (2019).
1484 The Splicing Factor hnRNP M Is a Critical Regulator of Innate Immune Gene Expression in
1485 Macrophages. Cell Rep *29*, 1594-1609 e1595.
1486